Journal of Computational Neuroscience 11, 63–85, 2001

Effects of Neuromodulation in a Cortical Network Model of Object Working Memory Dominated by Recurrent Inhibition

NICOLAS BRUNEL
LPS, Ecole Normale Supérieure, 24 rue Lhomond, 75231 Paris Cedex 05, France
brunel@lps.ens.fr

XIAO-JING WANG
Volen Center for Complex Systems, Brandeis University, 415 South St., Waltham, MA 02254-9110, USA
xjwang@volen.brandeis.edu

Received November 22, 2000; Revised April 13, 2001; Accepted April 13, 2001

Action Editor: Prof. M. Tsodyks

Abstract. Experimental evidence suggests that the maintenance of an item in working memory is achieved through persistent activity in selective neural assemblies of the cortex. To understand the mechanisms underlying this phenomenon, it is essential to investigate how persistent activity is affected by external inputs or neuromodulation. We have addressed these questions using a recurrent network model of object working memory. Recurrence is dominated by inhibition, although persistent activity is generated through recurrent excitation in small subsets of excitatory neurons.

Our main findings are as follows. (1) Because of the strong feedback inhibition, persistent activity shows an inverted U shape as a function of increased external drive to the network. (2) A transient external excitation can switch off a network from a selective persistent state to its spontaneous state. (3) The maintenance of the sample stimulus in working memory is not affected by intervening stimuli (distractors) during the delay period, provided the stimulation intensity is not large. On the other hand, if stimulation intensity is large enough, distractors disrupt sample-related persistent activity, and the network is able to maintain a memory only of the last shown stimulus. (4) A concerted modulation of $GABA_A$ and NMDA conductances leads to a decrease of spontaneous activity but an increase of persistent activity; the enhanced signal-to-noise ratio is shown to increase the resistance of the network to distractors. (5) Two mechanisms are identified that produce an inverted U shaped dependence of persistent activity on modulation. The present study therefore points to several mechanisms that enhance the signal-to-noise ratio in working memory states. These mechanisms could be implemented in the prefrontal cortex by dopaminergic projections from the midbrain.

Keywords: working memory, network model, prefrontal cortex, inferotemporal cortex, spontaneous activity, persistent activity, NMDA, GABA, AMPA, dopamine

1. Introduction

Neurophysiological studies of working memory have revealed that, when an animal must retain the memory of the identity of a visual object during a delay period between the stimulus and behavioral response, neurons show a selectively enhanced activity throughout the delay period, in prefrontal cortex (PFC) (Fuster and

Alexander, 1971; Kubota and Niki, 1971; Wilson et al., 1993), in inferotemporal cortex (ITC) (Fuster and Jervey, 1981; Miyashita, 1988; Miyashita and Chang, 1988) as well as in other areas of the temporal lobe (Nakamura and Kubota, 1995). More recent experiments have shown an important difference in delay activity between the PFC and ITC. Mnemonic activity is resistant to distractors in PFC but not in ITC (Miller et al., 1996).

It has long been hypothesized (Lorente de Nó, 1933; Hebb, 1949; Amit, 1995; Goldman-Rakic, 1995) that excitatory synaptic loops could sustain persistent neural activity, after a transient stimulus. Reverberatory excitations, however, presumably must be counteracted by feedback inhibition mediated by GABAergic interneurons (Condé et al., 1994; Kawaguchi, 1997; Gabbott and Bacon, 1996), for the control of network excitability. Synaptic inhibition is also likely to be critical for shaping the selectivity of mnemonic neural activity in a working memory circuit (Goldman-Rakic, 1995; Camperi and Wang, 1998; Rao et al., 1999; Compte et al., 2000), similarly to the tuning of neural responses in sensory cortices. In the context of working memory models, Amit and Brunel (1997) showed that, in order to reproduce experimental observations from the physiological studies of behaving monkeys, the network model should be dominated by inhibition, in the sense that recurrent excitatory-inhibitory synaptic interactions are overall balanced toward inhibition. However, little is known about the functional consequences of inhibition dominance, other than the regulation of network excitability.

Mnemonic neuronal activity is also believed to be controlled and dynamically modulated by neurotransmitters. In particular, dopamine has received in recent years a lot of attention due to its important role in working memory function (see Arnsten, 1998, for a recent review). Experiments with behaving monkeys have found that iontophoresis of a D1 dopamine receptor agonist in PFC produces an increase in persistent activity, while a D1 receptor antagonist has the reverse effect (Sawaguchi et al., 1990). Behavioral studies demonstrated that depletion of dopamine within the PFC (Brozoski et al., 1979), or infusions of D1 antagonists into the PFC (Sawaguchi and Goldman-Rakic, 1991), severely impairs working memory performance. There appears to be an optimal level of dopamine modulation, since high doses of D1 receptor agonists impaired working memory performance of aged monkeys (Cai and Anrsten, 1997) and rodents (Zahrt et al., 1997); and low doses of D1 receptor antagonists have been reported to increase delay-period activity in PFC neurons of behaving monkeys (Williams and Goldman-Rakic, 1995). Elucidating the neuronal basis of such modulatory processes is important to our understanding of cortical mechanisms of working memory, as well as working memory deficits associated with schizophrenia (Daniel et al., 1991; Goldman-Rakic, 1994; Okubo et al., 1997). Recent experiments have began to identify cellular and synaptic sites of dopaminergic action, but the exact effects of dopamine remain controversial. Dopamine D1 receptor activation was found to affect NMDA receptor mediated EPSPs in the PFC (Cepeda et al., 1992; Zheng et al., 1999; Law-Tho et al., 1994), as well as inhibitory synaptic transmission (Penit-Soria et al., 1987; Gellman and Aghajanian, 1993; Law-Tho et al., 1994). Moreover, DA reduces the amplitude of isolated dendritic Ca^{2+} spikes generated by a dendritic high-voltage-activated Ca^{2+} current (Yang et al., 1996), which might effectively reduce the amplitude of distal synaptic inputs. It is unclear how these in vitro observations may be related to the PFC function at the network level and thus to working memory of the behaving animals. The question is of clinical importance, since dysfunction of D1 receptor signaling is implicated in working memory deficits associated with schizophrenia (Goldman-Rakic, 1994; Okubo et al., 1997; Egan and Weinberger, 1997) and increase in dopamine levels by amphetamine improves working memory ability of schizophrenic patients (Daniel et al., 1991). It is therefore a major challenge to identify the mechanisms of dopaminergic action in prefrontal cortical networks. To this end, we need to understand how dopamine modulation of cellular and synaptic processes affects the collective behavior of a recurent cortical network.

Recently, Durstewitz and collaborators (1999, 2000) have investigated dopamine modulation of working memory in a network model of prefrontal cortex, using either simplified firing-rate models or models composed of a small number of biophysically detailed neurons. We have taken a similar approach, using computational modeling as a tool to help bridge the gap between slice data and neural mnemonic activity of behaving animals. In the present study, we focus on a model of a large cortical network of object working memory that is dominated by feedback inhibition, and we study the interplay between external inputs, neuromodulation, and recurrent inhibition. Similarly to Durstewitz et al., we find that a concomitant

enhancement of the NMDA receptor-mediated recurrent excitation and recurrent inhibition increases the delay-to-spontaneous activity (signal-to-noise) ratio and that this effect dramatically enhances the resistance of the network to distractors. However, we find two other mechanisms that lead to such an enhancement but only in a limited range of modulation: a reduction in background external inputs and a differential modulation of NMDA conductances on excitatory and inhibitory cells. In contrast to the NMDA/GABA modulation, these types of modulation lead to an inverted-U shape for the dependence of persistent activity on modulation strength, as is found in both electrophysiological and behavioral studies (Williams and Goldman-Rakic, 1995; Arnsten, 1998). We discuss possible implications of these results for dopaminergic modulation of working memory function.

2. Methods

2.1. The Cortical Module

The model combines a network architecture taken from Amit and Brunel (1997) and descriptions of synaptic currents from Wang (1999). The main features of the model are that (a) persistent activity is generated within a local cortical circuit, (b) recurrent synaptic excitation is largely mediated by NMDA receptors, and (c) recurrent network interactions are dominated by synaptic inhibition.

The network is composed of N_E pyramidal cells (80%) and N_I interneurons (20%) (Braitenberg and Schütz, 1991; Abeles, 1991). It represents a cortical module of an area receiving information about the identity of objects—inferotemporal cortex or ventral prefrontal cortex. Each neuron receives C_E excitatory synaptic contacts from pyramidal cells and C_I inhibitory contacts from interneurons. For simplicity, most simulations performed in this article are done using $N_E = C_E = 800$, $N_I = C_I = 200$ (fully connected network). Some simulations were performed with $N_E = C_E = 2000$, $N_I = C_I = 500$. Both pyramidal cells and interneurons also receive $C_{ext} = 800$ excitatory connections from outside the network. These connections send to the network all the information (stimuli) received from the outside world, as well as background noise due to spontaneous activity outside the module, that arrive at each external synapse with a rate of 3 Hz, which correspond to a typical value for spontaneous activity in the cerebral cortex (Burns and Webb, 1976; Koch and Fuster, 1989; Wilson et al., 1994). Since there are 800 external synapses, the total background external input to any cell of the network has a rate of $\nu_{ext} = 2.4$ kHz.

2.2. Neurons

Both pyramidal cells and interneurons are described by leaky integrate-and-fire neurons (see, e.g., Tuckwell, 1988) and are characterized by a resting potential $V_L = -70$ mV, a firing threshold $V_{thr} = -50$ mV, a reset potential $V_{reset} = -55$ mV, a membrane capacitance $C_m = 0.5$ nF for pyramidal cells, 0.2 nF for interneurons, a membrane leak conductance $g_m = 25$ nS for pyramidal cells, 20 nS for interneurons, and a refractory period $\tau_{rp} = 2$ ms for pyramidal cells, 1 ms for interneurons. The corresponding membrane time constants are $\tau_m = C_m/g_m = 20$ ms for excitatory cells and 10 ms for interneurons (McCormick et al., 1985). Below threshold, the membrane potential $V(t)$ of a cell

$$C_m \frac{dV(t)}{dt} = -g_m(V(t) - V_L) - I_{syn}(t),$$

where $I_{syn}(t)$ represents the total synaptic current flowing into the cell.

2.3. Synapses

There are four families of synapses: excitatory (glutamatergic) synapses on pyramidal cells and interneurons; inhibitory (GABAergic) synapses on pyramidal cells and interneurons. Recurrent excitatory postsynaptic currents (EPSCs) have two components, mediated by AMPA and NMDA receptors, respectively. In most simulations, external EPSCs were mediated exclusively by AMPA receptors. In a few simulations, we introduced NMDA receptors in external inputs. The total synaptic currents are given by

$$I_{syn}(t) = I_{AMPA,ext}(t) + I_{AMPA,rec}(t) + I_{NMDA,rec}(t) + I_{GABA,rec}(t)$$

in which

$$I_{AMPA,ext}(t) = g_{AMPA,ext}(V(t) - V_E) \sum_{j=1}^{C_{ext}} s_j^{AMPA,ext}(t)$$

$$I_{AMPA,rec}(t) = g_{AMPA,rec}(V(t) - V_E) \times \sum_{j=1}^{C_E} w_j s_j^{AMPA,rec}(t)$$

$$I_{\mathrm{NMDA,rec}}(t) = \frac{g_{\mathrm{NMDA}}\,(V(t)-V_{\mathrm{E}})}{(1+[\mathrm{Mg}^{2+}]\exp(-0.062V(t))/3.57)} \times \sum_{j=1}^{C_{\mathrm{E}}} w_j s_j^{\mathrm{NMDA}}(t)$$

$$I_{\mathrm{GABA,rec}}(t) = g_{\mathrm{GABA}}\,(V(t)-V_{\mathrm{I}}) \sum_{j=1}^{C_{\mathrm{I}}} s_j^{\mathrm{GABA}}(t),$$

where $V_{\mathrm{E}} = 0$ mV, $V_{\mathrm{I}} = -70$ mV. The dimensionless weights w_j represent the structured excitatory recurrent connections (see below); the sum over j represents a sum over the synapses formed by presynaptic neurons j. The NMDA currents have a voltage dependence that is controlled by the extracellular magnesium concentration (Jahr and Stevens, 1990), $[\mathrm{Mg}^{2+}] = 1$ mM. The gating variables or fraction of open channels s are described as follows. The AMPA (external and recurrent) channels are described by

$$\frac{ds_j^{\mathrm{AMPA}}(t)}{dt} = -\frac{s_j^{\mathrm{AMPA}}(t)}{\tau_{\mathrm{AMPA}}} + \sum_k \delta\big(t-t_j^k\big),$$

where the decay time of AMPA currents is taken to be $\tau_{\mathrm{AMPA}} = 2$ ms (Hestrin et al., 1990; Spruston et al., 1995), and the sum over k represents a sum over spikes emitted by presynaptic neuron j. In the case of external AMPA currents, the spikes are emitted according to a Poisson process with rate ν_{ext}, independently from cell to cell. The NMDA channels are described by

$$\frac{ds_j^{\mathrm{NMDA}}(t)}{dt} = -\frac{s_j^{\mathrm{NMDA}}(t)}{\tau_{\mathrm{NMDA,decay}}} + \alpha x_j(t)\big(1-s_j^{\mathrm{NMDA}}(t)\big)$$

$$\frac{dx_j(t)}{dt} = -\frac{x_j(t)}{\tau_{\mathrm{NMDA,rise}}} + \sum_k \delta\big(t-t_j^k\big),$$

where the decay time of NMDA currents is taken to be $\tau_{\mathrm{NMDA,decay}} = 100$ ms, $\alpha = 0.5$ ms^{-1}, and $\tau_{\mathrm{NMDA,rise}} = 2$ ms (Hestrin et al., 1990; Spruston et al., 1995). Last, the GABA synaptic variable obeys to

$$\frac{ds_j^{\mathrm{GABA}}(t)}{dt} = -\frac{s_j^{\mathrm{GABA}}(t)}{\tau_{\mathrm{GABA}}} + \sum_k \delta\big(t-t_j^k\big),$$

where the decay time constant of GABA currents is taken to be $\tau_{\mathrm{GABA}} = 10$ ms (Salin and Prince, 1996; Xiang et al., 1998). Note that we neglect the rise time of both AMPA and GABA currents, which are typically extremely short (<1 ms). All synapses have a latency 0.5 ms.

The synaptic coupling strengths were calibrated using the mean field analysis (see below and Appendix), such as to obtain desired levels of spontaneous activity. We used the following values for the recurrent synaptic conductances (in nS) in the 1000 neurons network: for pyramidal cells, $g_{\mathrm{AMPA,ext}} = 2.08$, $g_{\mathrm{AMPA,rec}} = 0.104$, $g_{\mathrm{NMDA}} = 0.327$ and $g_{\mathrm{GABA}} = 1.25$; for interneurons, $g_{\mathrm{AMPA,ext}} = 1.62$, $g_{\mathrm{AMPA,rec}} = 0.081$, $g_{\mathrm{NMDA}} = 0.258$, and $g_{\mathrm{GABA}} = 0.973$. Note that these synaptic conductances are about 1 nS in magnitude and therefore correspond roughly to experimentally measured conductances (see, e.g., Destexhe et al., 1998 and references therein). In the 2500 neurons network, all recurrent conductances were multiplied by 0.4. Two other points are noteworthy. First, recurrent excitation is assumed to be largely mediated by the NMDA receptors, since the network mnemonic activity is expected to be more stable when sustained by the slow NMDA-activated synapses (Wang, 1999). With our standard parameter set, the ratio of the NMDA over AMPA component of the unitary EPSC is about 0.08 in peak current but about 4.5 in terms of the charge entry at the resting membrane potential of −70 mV because of the much longer time course of the NMDA component. When the cell is near the firing threshold of around −55 mV, the ratio of NMDA:AMPA components becomes 10 in terms of charge entry, due to the partial relief of NMDA receptor channels from $[\mathrm{Mg}^{2+}]$ blockade. Second, the amplitude of recurrent excitation is smaller than that of inhibition (Amit and Brunel, 1997). The net recurrent input to a cell is therefore hyperpolarizing during spontaneous activity. This assumption has dramatic network implications (see Section 3, Results).

2.4. *External Stimuli*

The network is assumed to encode the identities of p object stimuli. Each of them activates a distinct and small subpopulation of fN_{E} excitatory cells, with $fp < 1$. Thus, external stimuli define p functional assemblies of fN neurons, each labelled by its preferred stimulus, and one population of $(1-fp)N$ neurons that do not respond to any of the stimuli. This classification of cells according to their selectivity properties is based on neurophysiological data from ITC or PFC of the monkey during delayed-response tasks. In these experiments, cells that are visually responsive to at least one of the shown pictures can be classified according to their best stimulus. Cells that do not show any

significant activation for any of the shown pictures can be classified in the nonselective group. In the following we use $p = 5$, $f = 0.1$.

2.5. *Structure of Recurrent Excitatory Connections Between Pyramidal Cells*

The coupling strength between a pair of neurons is prescribed according to a Hebbian rule: the synapse is strong (weak) if in the past the two cells tended to be active in a correlated (anticorrelated) manner. Hence, inside a selective population $w_j = w_+$, where $w_+ > 1$ is a dimensionless parameter that is equal to the relative strength of potentiated synapses with respect to the baseline. Unless specified otherwise, we used $w_+ = 2.1$. Between two different selective populations, and from the nonselective population to selective ones, $w_j = w_-$, where $w_- < 1$ measures the strength of synaptic depression. Other connections have $w_j = 1$. It is assumed that the spontaneous activity of neurons is largely unaffected by synaptic modifications because synaptic depression compensates the effect of potentiation at the network level. More specifically, by choosing $w_- = 1 - f(w_+ - 1)/(1 - f)$, the overall recurrent excitatory synaptic drive in the spontaneous state remains constant as w_+ is varied (Amit and Brunel, 1997). Synaptic efficacies remain fixed through the simulation.

Note that two possible scenarios would lead to such a connectivity structure in real cortical networks. In the first scenario, cells that are selective to a particular object would have no spatial relationship. In that scenario, the connectivity structure would be due to Hebbian learning (see, e.g., Brunel et al., 1998). Two cells firing together during the stimulus presentation would increase the strength of their connections, while long-term depression mechanisms would lead to weaker connections between cells selective to different stimuli. In the second scenario, the cells that are selective to the same stimulus would be close together, as perhaps in the same column. The connectivity structure would reflect the fact that the average distance between two cells selective for different objects is larger than between two cells selective for the same object, and thus the connection probability is smaller. Of course, the situation in the real cortex might be an intermediate one, with cells selective to a particular object tending to cluster in space, and connectivity structure is sharpened by learning processes. More experimental data are needed to distinguish between these scenarios. The cortical network is illustrated in Fig. 1.

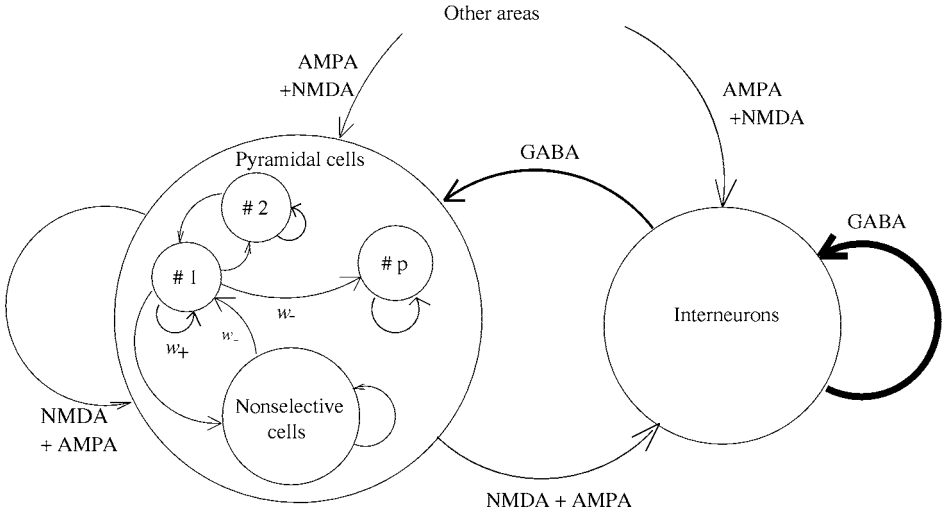

Figure 1. The cortical network model. Pyramidal cells (E cells) send connections to other pyramidal cells through AMPA and NMDA synapses. Interneurons (I cells) send GABAergic connections to pyramidal cells and other interneurons. Both receive excitatory connections from other cortical areas. Pyramidal cells can be functionally divided in several groups according to their selectivity properties. Group #1 is selective to object #1, etc. Cells within a group have relatively stronger connections (modulated by $w_+ > 1$), while connections between different groups are relatively weaker (modulated by $w_- < 1$). See Methods for more details.

2.6. Investigations of the Behavior of the Network

The model has been studied using both computer simulations and analytical techniques. We describe shortly in the following how both methods have been implemented. The Appendix gives all the details of the analytical techniques.

2.7. Simulations

Explicit simulations of the network of 1000 or 2500 neurons have been run on a Linux workstation, using a modified RK2 routine (Press et al., 1992; Hansel et al., 1998) for the numerical integration of the coupled equations describing the dynamics of all cells and synapses, with integration time step $dt = 0.1$ ms. External spike timings were generated randomly and independently inside each dt interval, and the s_{ext} variables at each cell were calculated exactly using these spike times, both at midstep and at the end of the step. Thes estimates were then used in the RK2 routine for updating other variables. The results of the simulations were shown to be independent of dt in the range 0.01 to 0.1 ms. We thus used $dt = 0.1$ ms in most simulations.

2.8. Analysis

In parallel, we have performed explicit mathematical calculations of the average discharge rates in each of the populations that define the network, as a function of neuronal, synaptic, and network parameters, using a generalization of analytical techniques introduced in Amit and Brunel (1997). The analysis allows us to determine in a self-consistent way the firing frequencies of each of the populations in stationary (asynchronous) states of the network, as a function of the model parameters. The situation of interest here corresponds to the delay period following the presentation of a stimulus that has been previously shown to the network. In this situation there are four functionally different populations of cells: cells belonging to the population that is selectively activated by the shown stimulus (this population is denoted by *act*); cells belonging to populations that are tuned to other stimuli (+); excitatory cells that are activated by none of the stimuli (0); and interneurons (I). Again, this classification in four populations corresponds to the phenomenology of neuronal mnemonic activity of behaving monkeys. Indeed, in delayed-response tasks, a recorded pyramidal cell can fall in one of three categories: either its best stimulus is the shown stimulus (population *act*); or its best stimulus is a different stimulus (population +); or the cell has no best stimulus (population 0). The mean-field analysis is described in detail in the Appendix.

3. Results

3.1. Network Behavior During a Delayed Match-to-Sample Simulation

The network was simulated using the following delayed-response protocol: (1) The simulation starts with a pre-cue time interval of 1 s, in which the network exhibits spontaneous activity. (2) Stimulus presentation (sample) consists of a transient input (lasting for 500 ms) to those cells selective to the shown stimulus. It is implemented by an increase in the input frequency from ν_{ext} to $\nu_{\text{ext}} + \lambda$, where λ represents the intensity of visual stimuli, and is typically a few tens of Hz. Other cells are unaffected. (3) After the external stimulus is removed, there is a delay period of 4 s. (4) Finally, a match stimulus is presented during 500 ms, using the same intensity λ. In the last 400 ms of the match presentation, the external frequency to *all cells* ν_{ext} is multiplied by 1.5 to account for an increase in afferent inputs due to the behavioral response/reward signal.

Figure 2A shows the basic behavior of the network during a particular simulated trial. The top panel shows the spike trains of 50 selected cells of the network: 4 selective to the shown stimulus (red); 4×4 selective to other stimuli (green, blue, yellow, and brown); 20 selective to none of the stimuli (cyan); and 10 interneurons (black). The bottom panel shows the average activity in each of these populations. Before sample presentation, all cells in the network are spontaneously active at rates of a few hertz. Pyramidal cells have an average spontaneous rate of 3 Hz, while interneurons have an average spontaneous rate of 9 Hz. These values are on the order of magnitude of average spontaneous rates as recorded extracellularly in prefrontal cortex (Wilson et al., 1994). The shown stimulus (red) elicits a strong transient response in the corresponding cells. Note that this strong response occurs even though the stimulus amplitude is relatively small (about 5% above background inputs). The sensitivity of the system to such small transient inputs is due to the fact that the network is not silent before stimulus presentation. Neurons are in a state of spontaneous activity, their membrane

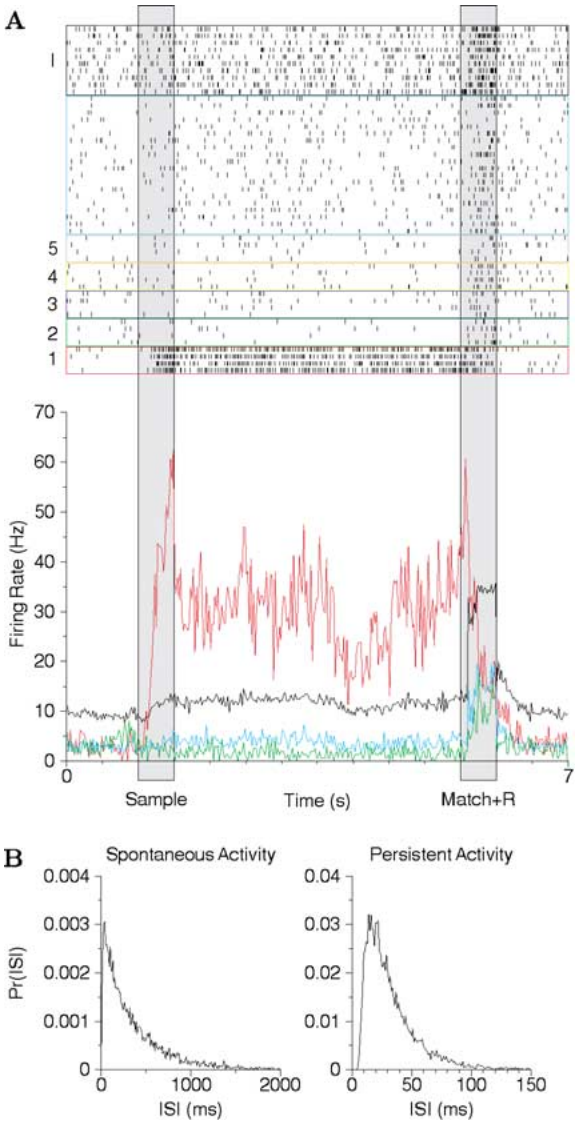

Figure 2. Selective persistent activity in a delayed match-to-sample simulation. **A:** Average activity of different populations and rastergrams of randomly selected cells. Red: cells selective for the shown stimulus. Green, yellow, blue, and brown: cells selective for other stimuli. Cyan: cells nonselective to any of the stimuli. Black: Inhibitory cells. The stimulus triggers persistent activity in a selective cell population (red) at about 25 Hz. Delay period activity is switched off by a transient excitatory input generating a brief surge of activity in all neurons. **B:** Interspike interval histograms of sample-selective cells in spontaneous and persistent activity. Note different time scales. Network of 1000 neurons, $w_+ = 2.1$.

potentials are just below threshold for action potential firing, due to a balancing of excitatory and inhibitory inputs (see below). These cells sustain their activity at about 25 Hz during the delay, while other cells remain at low levels of activity. Cells selective for other stimuli actually slightly decrease their activity compared to the spontaneous state. During the first 100 ms of the match presentation, the cells selective to the shown stimulus show a surge of activity. After that, a nonselective input is applied to all cells in the network (see the increase in the activity of all cells during the response period), which effectively wipes out the persistent activity of the red cells.

Figure 2B shows the interspike interval (ISI) histograms of cue-selective cells, in the spontaneous activity state (left) and in the working memory state (right). In the spontaneous activity state, the histogram is nearly perfectly exponential, with a coefficient of variation (CV) of the ISIs close to one. This means that the firing process of cells in the spontaneous activity state is close to a Poisson process. In the working memory state, the CV is slightly lower (about 0.7) but remains at a rather high value. Cells indeed keep firing very irregularly in that state, as can be seen by inspection of the rastergram shown in the upper panel.

3.2. *Inhibition Dominance of Recurrent Circuit*

The synaptic currents of various types received by a single cell are plotted in Fig. 3. Let us emphasize that those are the *time-averaged currents* during persistent neural discharges, not unitary postsynaptic currents elicited by a single spike. During spontaneous activity (top panel), cells receive a large amount of external current—that is, above the deterministic current threshold of spike discharges (>0.45 nA). However, since the sum of the recurrent AMPA and NMDA synaptic currents is smaller in amplitude than the GABA synaptic current (see the top panel), the feedback input is predominantly inhibitory. Therefore, the total (external plus recurrent) synaptic input is actually slightly subthreshold (<0.45 nA), and firing is primarily triggered by fluctuations in the input around the firing threshold. During the delay period (middle and bottom panels), cells that are tuned to the sample stimulus show a large increase of all the recurrent components (AMPA, NMDA, and GABA) due to an increase of activity in the selective population and in interneurons that are excited to fire at higher rates (middle panel). The total recurrent component becomes slightly excitatory due to strong recurrent synapses within the selected subpopulation, and the resulting total synaptic input turns out to be now slightly superthreshold. On the other hand, cells that have not been activated by the sample stimulus

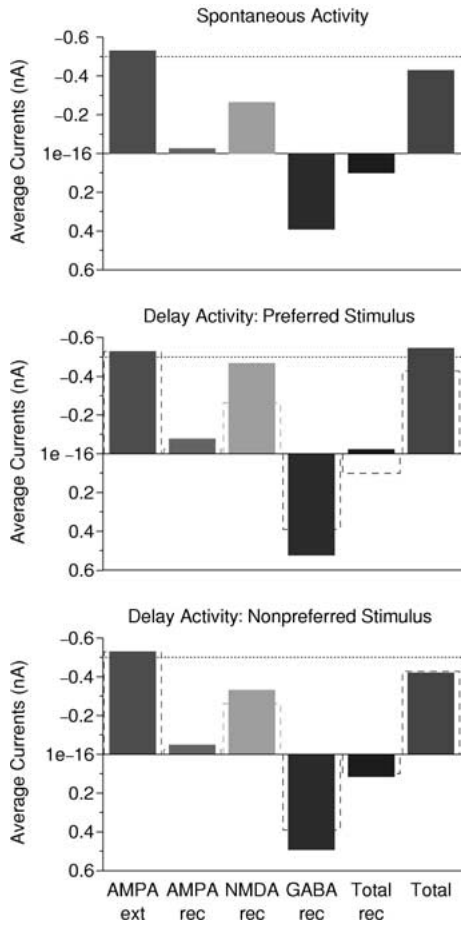

Figure 3. Synaptic mechanisms of working memory. Various components of synaptic current in a single cell during spontaneous activity (top), during delay activity following presentation of a preferred stimulus (middle), and during delay activity following presentation of a nonpreferred stimulus (bottom). The dotted line indicates the magnitude of excitatory synaptic currents needed to reach the deterministic threshold. In the two lower panels, the dotted boxes indicate the magnitude of the corresponding component during spontaneous activity, to emphasize the differences between delay and spontaneous activity. External inputs (AMPA ext) are superthreshold. The three components of recurrent connectivity (AMPA rec, NMDA rec, and GABA rec) indicate the relative strengths of each. Their sum gives the total recurrent inputs (total rec). Finally, the sum of external and total recurrent gives total. Note that the total recurrent inputs are hyperpolarizing during spontaneous activity, while they are slightly depolarizing in a memory state following presentation of the preferred stimulus. They are slightly decreased compared to spontaneous activity after presentation of a nonpreferred stimulus, due to enhanced inhibition.

show a relatively smaller recurrent AMPA and NMDA components, since the connections they receive from the selectively active cells are weak in strength. The resulting total recurrent input thus remains inhibitory, which results in a firing level close to spontaneous activity.

Note that the reverberation mechanism for sustaining selective persistent activity operates locally, within a cell subpopulation. It is thus compatible with inhibition dominance at the global network level.

Another feature of Fig. 3 is that the NMDA component is several fold larger than the AMPA component of the recurrent excitatory synaptic current. Contribution by the NMDA receptors is important to stably maintain persistent activity in a strongly recurrent circuit, as was shown previously with an unstructured network model (Wang, 1999) and with a spatial working memory model (Compte et al., 2000). This conclusion also holds with our structured network model of object working memory. In the opposite situation, if recurrent excitation is not dominated by the slow NMDA receptors, and AMPA-mediated excitation is much faster than feedback inhibition, the recurrent network dynamics tends to develop oscillatory instabilities (data not shown).

3.3. *Selective Persistent Activity by Structured Connectivity*

The network stores the memory of an object by persistent activity of a selective subpopulation of neurons. The network shows a *multistable* behavior: coexistence between a uniform spontaneous activity state and several persistent activity states (one for each stimulus stored in the synaptic structure). Transient inputs to the network can induce a transition between the spontaneous state and one of the persistent activity states.

This multistability emerges due to the structured strengthening of the excitatory connections and is present only for a finite range of the synaptic parameter w_+. In Fig. 4 are shown the firing rates of the spontaneous and persistent activities as a function of w_+, both for computer simulations and analytical calculations. The middle branch connecting the two represents an unstable state and thus is not directly observable. One sees that the coexistence between spontaneous activity and persistent activity states is present only in a finite range of w_+. With a too small w_+ value, recurrent synapses are not strong enough to generate and sustain elevated persistent activity in a neuronal assembly. On the other hand, if w_+ is too large, recurrent excitation becomes too strong and the low spontaneous state becomes

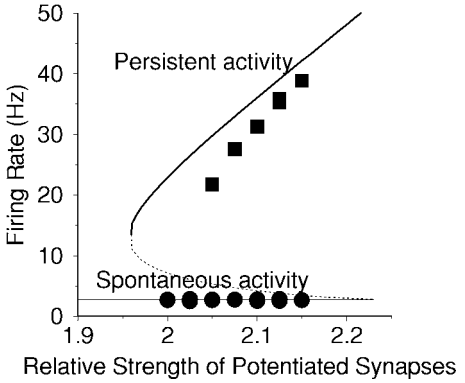

Figure 4. Dependence of network activity on the strength of potentiated synaptic connections. Bifurcation diagram showing firing rates in the stable states of the network versus w_+, measuring the structured potentiation of the recurrent excitatory connectivity: spontaneous activity and persistent memory activity. Unstable states are shown with dashed line. Filled circles: simulation results (2500 neurons); lines: analytical results from the mean-field equations (see Appendix).

unstable and disappears. Below $w_+ \sim 2.25$, spontaneous activity remains constant as w_+ is varied. This is due to the fact that the *average* excitatory synaptic efficacy remains constant, as we choose w_- to balance the potentiated synapses. Moreover, persistent activity increases with w_+ because the excitatory feedback within a selective population is directly proportional to w_+. The spontaneous and persistent states are separated by the unstable state (middle branch, dashed line in Fig. 4). The network is expected to converge to the spontaneous state (resp. persistent state) if it is initially below (resp. above) the unstable state. As w_+ increases, the difference in firing rate between the unstable state and persistent state (resp. spontaneous state) increases (resp. decreases). The persistent state becomes more stable at the expense of the spontaneous state, until spontaneous activity destabilizes when $w_+ \sim 2.25$.

Note that the spontaneous firing rates predicted by the mean-field analysis agree well with the simulation results. For persistent activity, although the general trend is correctly predicted, the mean-field calculation gives a consistently higher firing rate than the computer simulation. This discrepancy may be due to the approximations made for the mean-field analysis (see the Appendix).

In a finite network, both spontaneous and persistent activity states are not truly stable, in the sense that after a very long time external noise might provoke transitions towards different states. For example, if one waits for long enough, random fluctuations might provoke transitions from the spontaneous activity state to one of the memory states, and vice versa. When w_+ is not very close to the boundaries of the multistability range, the lifetimes of both states are typically very long (larger than several seconds).

3.4. *Effect of Nonspecific External Drive: A Mechanism to Switch Off Persistent Activity*

In Fig. 2, a transient *excitatory*, rather than inhibitory, input was used at the end of the delay period to switch the network from an elevated persistent state back to the baseline spontaneous state. Neuronal response to the match stimulus corresponds to a transient *increase* in neuronal firing, in agreement with experimental observations in PFC (see, e.g., Funahashi et al., 1989). Intuitively, this is possible because the recurrent network is dominated by inhibition. A strong transient and nonspecific excitation leads to the recruitment of sufficiently powerful recurrent inhibition that eventually brings the network back to the spontaneous state, thereby providing a mechanism for memory erasure.

In the absence of this component, persistent activity correlated with the sample presentation would survive the match and response periods, and memory activity could persist for long time, until an unusually high fluctuation brings the network back to spontaneous activity.

To understand more precisely the nature of this phenomenon, we show in Fig. 5 how spontaneous and persistent activity vary when the magnitude of the external drive (to both pyramidal neurons and interneurons) is varied. It shows again a finite range of multistability. Not surprisingly, spontaneous activity increases as the external input is increased. On the other hand, persistent activity is present only in a finite range of external drive. Unlike Fig. 4, in Fig. 5 the persistent state and unstable state branches form a closed curve. Depending on the value of w_+, the shape of the closed curve is either a mushroom or an isola according to the mathematical theory of dynamical systems (Murray, 1993). In either case, with increasing external drive, there is initially a slight increase in persistent activity level in a narrow external drive range where spontaneous activity is very low. Then, and in most of the range, persistent activity *decreases* as external drive increases. This seemingly paradoxical effect is due to the contradictory effects of external excitatory inputs and recurrent inhibition.

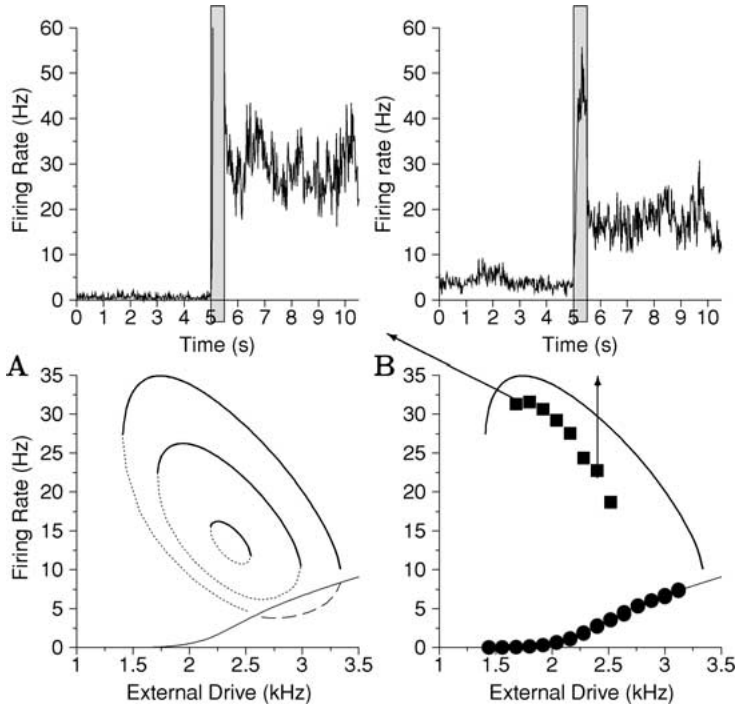

Figure 5. Modulation of network activity by external drive. Bifurcation diagram showing firing rates in the stable states of the network vs external drive to all cells of the network: Spontaneous activity and persistent memory activity. **A:** Bifurcation diagrams from mean-field equations. Thin line: spontaneous activity. Thick line: stable branch of the persistent activity curve, for three values of $w_+ = 1.96$, 2, 2.05. Increasing w_+ increases persistent activity, as in Fig. 4. Dotted line: unstable branch of the persistent activity. The branch of persistent state shows a mushroom for large w_+ (2.05) and an isola for small w_+ (1.96,2). **B:** $w_+ = 2.05$. The mean-field predictions are compared with the results of simulations of the network of 2500 neurons. Filled circles: spontaneous activity. Filled squares: persistent activity. Note that for most of the range in which persistent activity exists, decreasing the external drive decreases spontaneous activity, while the persistent activity level increases, so that the signal-to-noise ratio is enhanced. The two panels on top of the bifurcation diagrams show simulations performed at two levels of external drive, indicated by the arrows.

For small external inputs, spontaneous activity in both pyramids and interneurons is small, and therefore the effects of external inputs dominates. Thus, initially, persistent activity increases with the increase in external inputs. However, as activity in interneurons increases, inhibitory feedback inputs increase. In particular, the increase in shunting inhibition effectively act as a reduction of the feedback excitation. Above a critical value of external bombardment, this effect becomes larger than the increase in external excitation. Thus, after persistent activity reaches a maximum, it decreases with increasing external inputs. Thus, persistent activity destabilizes if the external inputs are sufficiently increased, as shown in Fig. 5. It can also be destabilized by a sufficient decrease in external inputs, leading to an almost completely silent network. Surprisingly, a decrease in the external inputs increases the delay-to-spontaneous activity (signal-to-noise) ratio in a wide range of input intensity, due to the combined decrease in spontaneous activity and increase in selective persistent activity.

3.5. *Memory Retention in the Presence of Distractors*

In order to investigate whether the network can preserve the memory of the sample stimulus in spite of interfering disturbances, model simulations were performed with distraction stimuli. We chose a simulation protocol similar to the distractor experiments of Miller et al. (1996). The set of used distractors was identical to that of sample stimuli, a stimulus used as distractor in one simulation could be the sample stimulus in another run. A distractor is a nonmatch stimulus different from the initial sample, applied to the subpopulation of

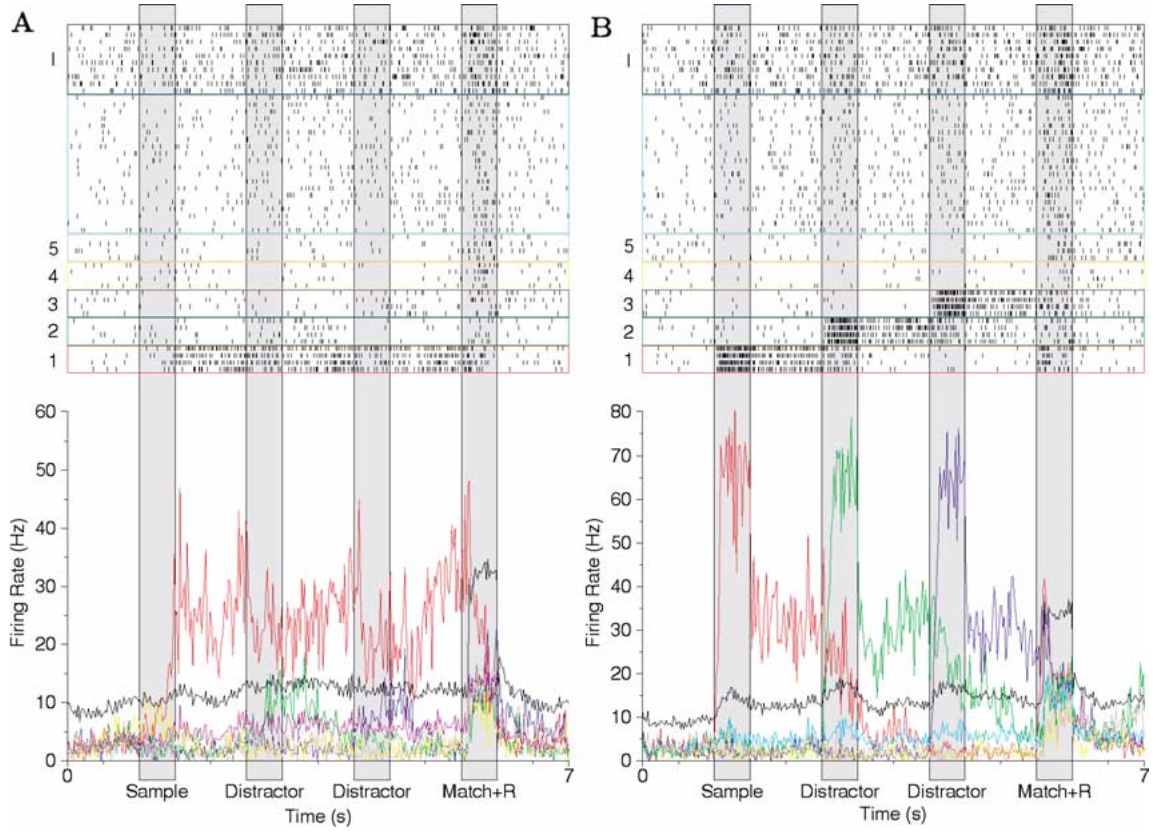

Figure 6. Delayed match-to-sample simulation with distractor stimuli. The sample stimulus (item 1) elicits selective persistent activity in the first neural subpopulation. Distraction stimuli (items 2 and 3) are sequentially presented during delay period. **A:** Sample-specific persistent activity is resistant to distractors at intermediate stimulus intensities ($\lambda = 60$ Hz) even though distractor stimuli provoke visual response. The memory storage for the sample-stimulus is preserved throughout the delay period. **B:** Sample-specific persistent activity is disrupted by distractors when stimulus intensity is high enough ($\lambda = 120$ Hz). Each distractor is strong enough to reset the network to a new persistent activity state corresponding to the latest shown stimulus. Network of 1000 neurons, $w_+ = 2.1$.

neurons selective to the distractor. Typically, in a simulation two distractors are shown consecutively during the delay period. The selective inputs due to distractors have the *same amplitude* as the sample and match stimuli (Fig. 6). We found that the effect of distractors on network activity depends mainly on the stimulus amplitude. At very weak stimulus intensity (λ less than about 40 Hz), presentation of the sample stimulus was unable to elicit any elevated delay activity. For intermediate values of stimulus amplitude (λ between 40 and 60 Hz) the sample stimulus elicited persistent activity that was then resistant to distractors (Fig. 6). This is due to the fact that inhibitory inputs to all cells of the network are higher during the delay than during spontaneous state, and the firing rates of cells not selective to the sample stimulus are lower than in the spontaneous state. It is therefore harder for external inputs to bring these neurons to their high activity state during the delay period than during the spontaneous state. For high values of stimulus amplitude (λ more than 60 Hz), cue-related persistent activity (short-term memory) is disrupted by the nonmatch stimuli and the network is distracted (Fig. 6). In this case, a nonmatch stimulus is sufficiently powerful to bring its corresponding neuronal assembly (whose best stimulus is the distractor) from a low firing state to its high firing state. Note that during the distraction stimulus there is *no* input directly applied to the initial neuronal subpopulation whose persistent activity is disrupted. These cells are turned off as a dynamical consequence of the rise of the new neuronal subpopulation, which leads to a transient surge of feedback inhibition to the rest of the network (see inhibitory population's firing rate during the distraction stimuli in Fig. 6).

Therefore, our simulations show that the network's ability of preserving short-term memory storage against distractors depends on two major factors: its inhibitory synaptic circuit and the amplitude of information-specific inputs.

3.6. Modulation by Neurotransmitters

We have shown above that the working memory network operation critically depends on the interplay between recurrent synaptic excitation mediated by NMDA receptors and inhibition mediated by $GABA_A$ receptors. We next examine how modulation of the NMDA and $GABA_A$ conductances affects the collective behavior of the network.

As expected, an increase in g_{GABA} leads to a decrease of the activity levels of both memory and spontaneous states, until the memory states disappear (Fig. 7A). Conversely, if g_{GABA} is decreased, memory and spontaneous rates increase, up to a point where the spontaneous activity state destabilizes. On the other hand, an increase in g_{NMDA} leads to an increase in both spontaneous and memory activity, until spontaneous activity destabilizes; and a decrease in g_{NMDA} reduces both rates, until memory activity disappears (Fig. 7B).

Figure 7C shows what happens when NMDA and GABA conductances are modulated together, with the same proportional change. An increase in both conductances leads to an increase in memory activity but to a decrease in spontaneous activity, leading to an increase in the signal-to-noise ratio. This is because, in the working memory state, elevated persistent activity induces a high recurrent excitatory drive in the selective neural subpopulation, so that the increase in inhibition is more than compensated by that in NMDA receptor mediated excitation. Therefore, the modulation of the GABA conductance predominates in the spontaneous activity state, while the modulation of the NMDA conductance predominates in the working memory state. Note also that the memory and spontaneous activity states now coexist in a much wider range than in the case of modulation of NMDA or GABA conductance alone (compare Fig. 7C with 7A and 7B). This effect also holds when NMDA receptors are included in the external inputs.

If modulatory manipulation is done locally on a single cell rather than globally to the network, an increase of both NMDA and GABA conductances leads to a *decreased* rather than increased persistent activity (Fig. 8). This is because, at the single-neuron level,

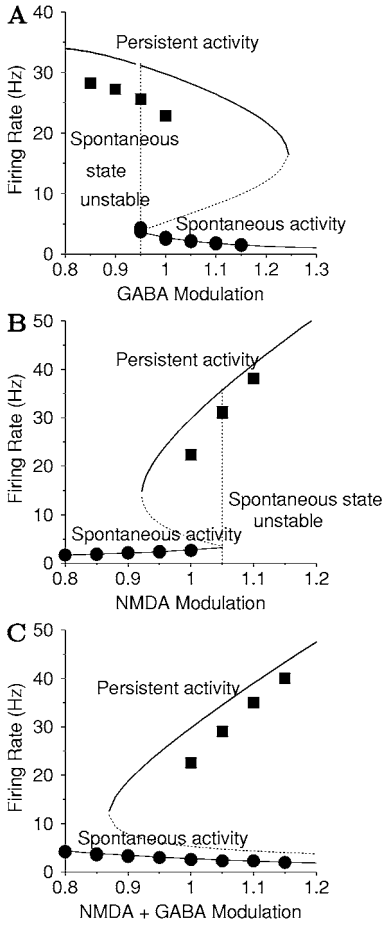

Figure 7. Modulation of MNDA receptor and $GABA_A$ receptor mediated synaptic transmissions. **A:** An increase in the GABA conductance of recurrent inhibition reduces both the spontaneous and persistent activities. **B:** An increase in the NMDA conductance of recurrent excitation increases both the spontaneous and persistent activities. **C:** A concomitant modulation of NMDA and GABA conductances, with the same dosage dependence, leads to a decrease of spontaneous activity and an increase of persistent activity, thereby enhancing the delay-to-spontaneous activity ('signal-to-noise') ratio. Unstable states are shown with a dashed line. Simulation results obtained with 2500 neurons. $w_+ = 2.05$.

the average synaptic current is somewhat larger in amplitude for the $GABA_A$ receptor-mediated inhibition than for the NMDA receptor mediated excitation (see Fig. 3). Thus, for a same proportional increase the effect of the GABA conductance is typically larger than that of the NMDA conductance, which results in a decrease of recurrent inputs to the cell. Hence, the effect of modulation of both the NMDA and GABA conductances on working memory activity is sensitive to how the modulation is done: a local increase leads

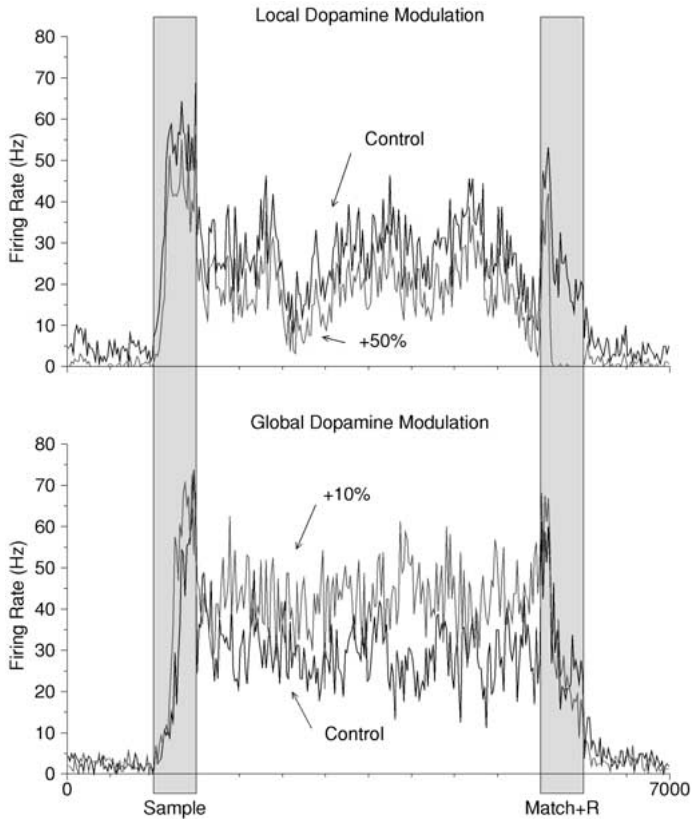

Figure 8. Local versus global modulation of the MNDA and $GABA_A$ synaptic conductances. Upper panel: A 50% increase in the GABA and NMDA conductances locally in a single cell reduces its persistent activity level. Lower panel: A 10% increase in the GABA and NMDA conductances globally for the entire network increases the persistent activity level of the same neuron. Network of 1000 neurons, $w_+ = 2.1$.

to a deterioration of working memory activity, while a global increase leads to an enhancement.

We have shown that a concerted increase in both NMDA and GABA conductances increases the signal-to-noise by increasing the difference between persistent activity and spontaneous activity. We then asked the question whether this modulation could enhance the network's resistance to distractors in a working memory state. To quantitatively address this issue, we varied systematically the level of simultaneous modulation of the NMDA and GABA conductances (like in Fig. 7C). For each level, we performed simulations with several values of the stimulus amplitude to determine the two amplitude thresholds separating the three regions of the stimulus amplitude: (1) weak stimulus that is incapable of switching on the network, (2) moderate stimulus that leads to the cue-related persistent activity robust against distractors, and (3) strong stimulus for which the memory of the cue can be disrupted by distractors.

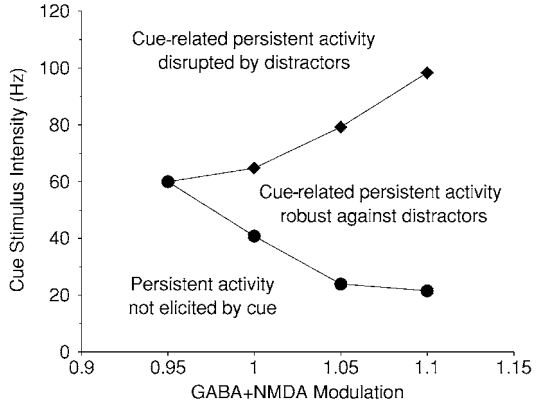

Figure 9. Robustness of cue-related persistent activity with respect to distractors, as a function of modulation of both NMDA and GABA conductances. Increasing the delay-to-spontaneous ratio expands greatly the range of cue stimulus intensity for which the cue-related persistent activity is resistant against distractors. Network of 1000 neurons, $w_+ = 2.1$.

The results are summarized in Fig. 9, where the x-axis corresponds to the modulation level of synaptic conductances, while the y-axis corresponds to stimulus amplitude. As one can see, the range of stimulus amplitude for which the network is resistant to distractors is very sensitive to the synaptic modulations (the range can increase almost fourfold when both conductances are increased by only 10%). This finding shows that the network's ability of robust memory storage against distractors can be greatly enhanced by moderate and concomitant modulation of recurrent NMDA receptor-mediated excitation and $GABA_A$ receptor-mediated inhibition.

We also examined the hypothesis that dopamine D1 receptor modulation could differentially affect pyramidal cells and interneurons because of the different sensitivities to dopamine levels of NMDAR channels in the two cell types (Muly et al., 1998). This was implemented by assuming that the NMDA conductances on pyramidal cells and those on interneurons are modulated by different levels of D1 activation. Specifically, we multiplied g_{NMDA} by a sigmoid function with a different threshold for pyramidal cells and interneurons (Fig. 10). As can be seen on the figure, at intermediate modulation levels, NMDA conductances in pyramidal cells are more affected than those in interneurons, giving a window of opportunity for delay activity to be enhanced. At higher activation levels, modulation of NMDA conductances on pyramidal cells saturates, a further increase in modulatory action now results in an increase of NMDA conductances on interneurons, and delay activity decreases and then disappears.

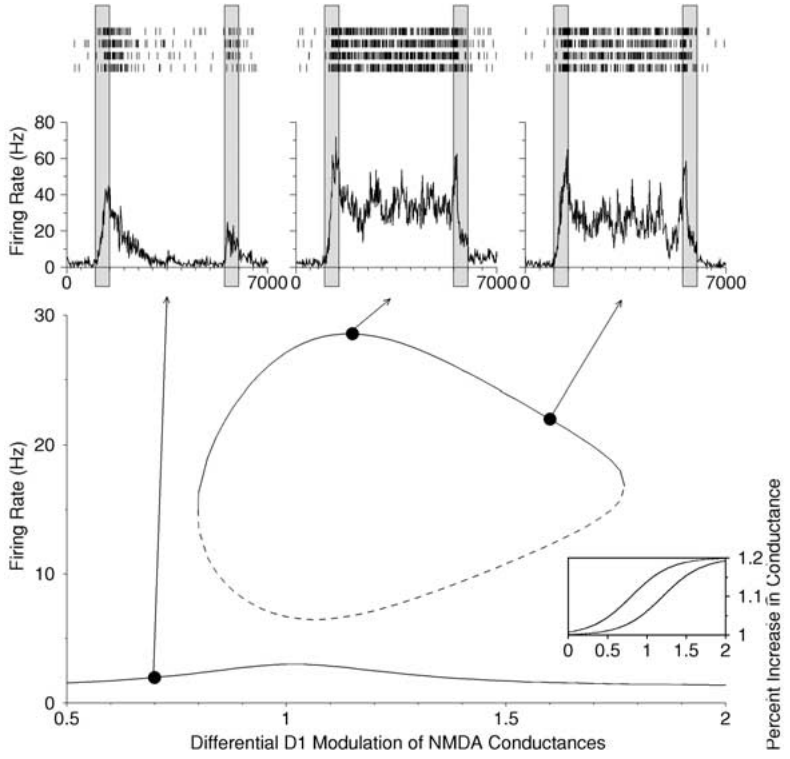

Figure 10. Differential dopamine D1 modulation of NMDA conductances in pyramidal neurons and interneurons following Muly et al. (1998). The bifurcation diagram shows that persistent activity is the highest in an intermediate range of D1 modulation. NMDA conductances on pyramidal cells are multiplied by a factor $c_E(1+0.2/(1+\exp((0.8-D_1)/0.25)))$, and those on interneurons are multiplied by $c_I(1+0.2/(1+\exp((1.2-D_1)/0.25)))$, where D_1 is the relative change of simulated D1 activation (compared to normal $D_1=1$ corresponding to the control parameter set, x-axis), and the constants c_E and c_I are chosen so that both factors are equal to 1 when $D_1=1$ (corresponding to the control parameter set). These two sigmoid curves are shown in the interest (lower right). Three simulations at different levels of D1 modulation indicated by filled circles are shown in the upper panels, showing that too high (right panel) or too low (left panel) D1 activation would be suboptimal or detrimental to working memory behavior. Compare with Williams and Goldman-Rakic (1995). $w_+ = 2.1$. Simulation results: network of 1000 cells.

Figure 10 shows that this scenario indeed gives rise to a bell-shaped curve for persistent activity. Spontaneous activity is less affected than delay activity but also shows a peak at moderate activation levels. Therefore, a differential modulation of NMDA receptor-mediated synaptic transmissions in pyramidal cells and interneurons naturally give rise to the inverted-U shape dependence on D1 activation of the working memory behavior (Arnsten, 1998).

The shape of the bifurcation diagrams remains qualitatively the same, when the modulation was done with the inclusion of NMDA receptors at external inputs.

4. Discussion

The balance between recurrent excitation and recurrent inhibition in cortical networks has been recently the subject of several theoretical studies (see, e.g., Shadlen and Newsome, 1994; Tsodyks and Sejnowski, 1995; van Vreeswijk and Sompolinsky, 1996; Amit and Brunel, 1997). In sensory cortices, some models of information processing emphasize the role of recurrent excitation (Somers et al., 1995; Douglas et al., 1995), while others suggest a predominant role for feedback inhibition (Pinto et al., 1996; Troyer et al., 1998). Here, we examined the operation of recurrent inhibition in a mnemonic network, using an object working memory model of spiking neurons coupled with realistic synapses. In this model, even though persistent activity in a subpopulation of neurons is sustained by excitatory reverberations, the recurrent circuit is overall dominated by feedback inhibition (see Fig. 3). In the inhibition dominance regime, the network model is capable of reproducing both spontaneous and stimulus-selective persistent activity with firing rates within physiological ranges in a delayed match-to-sample paradigm, as had been found in a simpler model (Amit and Brunel, 1997). Strong synaptic inhibition provides mechanisms for both memory erasure by transient excitatory inputs and robust resistance of the network to distractors.

4.1. *Switch-Off of Persistent Activity by Transient Increase of External Inputs*

Our study suggests a simple way of switching the network from a selective persistent activity state back to the spontaneous state: a brief increase in nonspecific afferents to all cells in the network, possibly due to reward or motor signals. Thus, our model predicts that the average firing rate of pyramidal cells during or just after the reward or motor response should increase transiently. Note that in this study we did not address the specific neuronal substrate of the switch-off signal. Moreover, whether memory is refreshed at the end of each delay period may depend on the behavior demand. In a study of delay activity in inferotemporal cortex (ITC), Yakovlev et al. (1998) showed that delay activity survives the test stimulus and persists until the next sample stimulus is presented.

4.2. *Effects of Intervening Stimuli on Persistent Activity*

Experimental studies show that cue-selective delay activity is disrupted by distractors in ITC, while it is preserved in PFC (Miller et al., 1996). Our network model has been shown to be resistant to distractors, provided that selective external inputs are not too strong to override recurrent synaptic actions. Note that our model does not require an additional mechanism to preserve the memory of the cue during distractor presentation, in contrast to Durstewitz et al. (1999), who assumed that the cue stimulus triggers a dopamine signal, which effectively shuts down external inputs, and thus distractors, during the delay period.

Our study raises the question whether the qualitative difference between ITC and PFC might be explained by the relative proximity to primary sensory areas. ITC, being closer to primary visual cortex, could be likely to receive a stronger intensity of selective input during cue presentation than PFC. It would be therefore natural to expect a stronger resistance to distractors in PFC. However, PFC responses during cue presentation are not smaller than those in IT cells (Miller et al., 1996). Alternatively, regional differences might originate from the differences in the synaptic circuitry and its dopaminergic modulations (see below).

4.3. *Mechanisms to Enhance the Signal-to-Noise Ratio and Possible Relationships with Dopamine*

It has been suggested that catecholamines, dopamine in particular, enhances the signal-to-noise ratio of mnemonic neuronal activity in the PFC (Servan-Schreiber et al., 1990; Sawaguchi et al., 1990). Delay

activity was found to have a bell-shaped curve in response to activation of D1 receptors (Williams and Goldman-Rakic, 1995). Behavioral data on both rats (Zahrt et al., 1997) and aged monkeys (Cai and Anrsten, 1997) have also demonstrated that there is an optimal level of D1 modulation for working memory performance. Durstewitz et al. (1999) explored dopamine modulation of the signal-to-noise ratio in a model where the dopamine system interacts with the prefrontal network in a reciprocal loop, and dopamine cells display elevated persistent activity during delay period. In a later paper, Durstewitz et al. (2000) considered *tonic* dopamine modulation of various synaptic currents and intrinsic ionic channels, in a Hodgkin-Huxley-type model of working memory. They showed that dopamine action could indeed increase the signal-to-noise ratio of a working memory circuit, therby enhancing the robustness of memory storage against distractors.

The present study differs from that of Durstewitz et al. (2000) in several respects. First, our network model is dominated by feedback inhibition, which leads to unique properties of network responsiveness to neuromodulation. Moreover, we have identified three distinct mechanisms that effectively enhance the signal-to-noise ratio and resistance to distractors. Finally, two of these mechanisms lead to an inverted U (bell-shaped) curve for the dependence of mnemonic activity on dopamine modulation.

The first mechanism leading to an increase in the delay-to-spontaneous activity ratio involves a decrease in external inputs (Fig. 5). There is evidence that dopamine reduces a dendritic high voltage-activated Ca^{2+} current that amplifies EPSPs in the distal dendrites (Yang et al., 1996). Since there is also evidence that afferent fibers from other cortical areas terminate in the upper PF cortex layers (Goldman-Rakic, 1987), it is reasonable to expect that external inputs will be the primary targets of such an effect. In that view, dopamine would reduce the external inputs received by the neuron (Durstewitz et al., 1999, 2000). We have shown, quite unexpectedly, that such a reduction would typically lead to a decrease in the spontaneous activity but an increase in the persistent activity. This happens because the intrinsic network is overall dominated by synaptic inhibition. Consequently, the delay-to-spontaneous activity ratio is increased in a wide range of modulation, and that delay activity would have an inverted U, or bell-shaped, curve in response to such a modulation. Such an effect could therefore be a candidate for an explanation to the role of dopamine in working memory processes.

The second mechanism found here involves an increase in both NMDA and GABA conductances (Fig. 7). Such a combined modulation leads to a decrease in spontaneous activity and an increase in delay activity, thereby increasing the signal-to-noise ratio. We found that if the recurrent network is dominated by inhibition, the effect is the opposite (a reduction of the persistent activity) if the modulation is done locally in a single cell (Fig. 8). If this is true, then local iontophoresis of drugs (Williams and Goldman-Rakic, 1995) that presumably affects only a few cells might not be adequate to probe dopamine modulation at the network level. Some in vitro experiments indicate that dopamine increases, at least in some concentration range, NMDA conductances in the PFC (Cepeda et al., 1992; Zheng et al., 1999) and that this effect is mediated by D1 receptors. A similar effect was found in the striatum (Umemiya and Raymond, 1997; Cepeda and Levine, 1998; but see Nicola et al., 2000). Law-Tho et al. (1994), however, found a decrease in NMDA conductance mediated by D1. The effects of dopamine on GABA are also a matter of debate. Several studies suggest that dopamine enhances the membrane excitability of GABAergic interneurons (Penit-Soria et al., 1987; Zhou and Hablitz, 1999), while Law-Tho et al. (1994) report a decrease of GABA conductances due to dopamine. Further studies are clearly needed to resolve the debate. Our modeling study indicates that a combined increase in NMDA and GABA conductances could lead to a considerable increase in signal-to-noise ratio, but the effect in delay activity would be monotonous, instead of the bell-shaped curve obtained with modulation of external inputs.

A third possible scenario that involves only the effect of dopamine D1 activation on NMDA receptors has been proposed recently. Muly et al. (1998) proposed that dopamine is effective on pyramidal cells at lower DA concentrations than on interneurons, raising the possibility that there is a concentration range in which NMDA conductances are substantially more enhanced on pyramidal cells than on interneurons. If D1 activation is too small, NMDA receptor mediated excitation would be too weak to sustain persistent activity; if it is too large, its action on pyramidal cells receptors saturates and the net effect is an enhanced inhibition. Thus, there is an optimal range of D1 modulation, leading to bell-shaped curve for the dependence of mnemonic activity on D1 modulation.

Our model confirmed that a differential modulation of NMDA conductances can indeed lead to an inverted-U shaped dose-dependent curve for persistent activity. An increase in the delay-to-spontaneous activity ratio, as could be accomplished by D1 receptor activation, leads to an dramatic enhancement of the network ability to sustain working memory in the advent of intervening stimuli (distractors). In light of this result, D1 modulation, though not strictly necessary to preserve the memory of a cue signal, might be helpful to increase the range of stability of the working memory states against distractors.

Appendix: Mean-Field Analysis of a Cortical Network Model for Object Working Memory

Mean-field analysis of networks of neurons with simplified synaptic inputs have been performed by Amit and Brunel (1997); Brunel and Sergi (1998); Brunel (2000). In this appendix, we generalize the analysis to networks of neurons that have conductance-based synaptic inputs. Along the way, several difficulties will be encountered. In some cases, these difficulties can be solved analytically. To do this, we need to perform some approximations whose logic and accuracy are described in the following.

Spontaneous Activity

The starting point of the analysis is the equation for the dynamics of a single pyramidal cell,

$$\begin{aligned} C_{\mathrm{m}}\frac{dV(t)}{dt} = & -g_{\mathrm{m}}(V(t)-V_{\mathrm{L}}) \\ & -g_{\mathrm{AMPA,ext}}(V(t)-V_{\mathrm{E}})\sum_{j=1}^{C_{\mathrm{ext}}} s_j^{\mathrm{AMPA,ext}}(t) \\ & -g_{\mathrm{AMPA,rec}}(V(t)-V_{\mathrm{E}}) \\ & \times \sum_{j=1}^{C_{\mathrm{E}}} w_j s_j^{\mathrm{AMPA,rec}}(t) \\ & -\frac{g_{\mathrm{NMDA}}(V(t)-V_{\mathrm{E}})}{1+\gamma\exp(-\beta V(t))}\sum_{j=1}^{C_{\mathrm{E}}} w_j s_j^{\mathrm{NMDA}}(t) \\ & -g_{\mathrm{GABA}}(V(t)-V_{\mathrm{I}})\sum_{j=1}^{C_{\mathrm{I}}} s_j^{\mathrm{GABA}}(t) \end{aligned} \quad (1)$$

where most variables are defined in the Methods section, except $\gamma = [\mathrm{Mg}^{2+}]/3.57$ and $\beta = 0.062$. We assume in the following that the network is in a stationary state in which population-averaged quantities, such as population frequencies and population-averaged synaptic currents, are constant.

In the diffusion approximation (see, e.g., Tuckwell, 1988), the sums of the synaptic variable s appearing in the right-hand-side of Eq. (1) can be replaced by an average DC component and a fluctuation term. In a spontaneous activity state, the network can be reduced functionally to two populations only, one of pyramidal cells, with discharge rate ν_{E}, one of interneurons, with discharge rate ν_{I}. The total synaptic variables of a pyramidal cell can therefore be written

$$\begin{aligned} S_{\mathrm{AMPA,ext}}(t) &\equiv \sum_{j=1}^{C_{\mathrm{ext}}} s_j^{\mathrm{AMPA,ext}}(t) \\ &= C_{\mathrm{ext}}\tau_{\mathrm{AMPA}}\nu_{\mathrm{ext}} + \Delta S_{\mathrm{AMPA,ext}}(t) \end{aligned} \quad (2)$$

$$\begin{aligned} S_{\mathrm{AMPA,rec}}(t) &\equiv \sum_{j=1}^{C_{\mathrm{E}}} w_j s_j^{\mathrm{AMPA,rec}}(t) \\ &= C_{\mathrm{E}}\tau_{\mathrm{AMPA}}\nu_{\mathrm{E}} + \Delta S_{\mathrm{AMPA,rec}}(t) \end{aligned} \quad (3)$$

$$\begin{aligned} S_{\mathrm{NMDA}}(t) &\equiv \sum_{j=1}^{C_{\mathrm{E}}} w_j s_j^{\mathrm{NMDA}}(t) \\ &= C_{\mathrm{E}}\psi(\nu_{\mathrm{E}}) + \Delta S_{\mathrm{NMDA}}(t) \end{aligned} \quad (4)$$

$$\begin{aligned} S_{\mathrm{GABA}}(t) &\equiv \sum_{j=1}^{C_{\mathrm{I}}} s_j^{\mathrm{GABA}}(t) \\ &= C_{\mathrm{E}}\tau_{\mathrm{GABA}}\nu_{\mathrm{I}} + \Delta S_{\mathrm{GABA}}(t), \end{aligned} \quad (5)$$

where the first term in the right-hand side of Eqs. (2) to (5) represent the DC component of the synaptic bombardment, while the second term represent the fluctuations around that DC component due to random arrival of spikes. Note that all DC components depend linearly on the presynaptic population discharge rate, except the NMDA component, which, due to nonlinear summation, has a nonlinear dependency in the pyramidal cell discharge rate, described by the function $\psi(\nu)$.

Approximation 1: Fluctuations Around the Mean Current. An approximation can be done considering the different noise terms ΔS in Eqs. (2) to (5). These noise terms are complicated to treat because each term has different temporal correlations, due to the different synaptic time constants of the synaptic receptors. However, a simple approximation can be made by noting that the time constant of AMPA receptors is much smaller than that of GABA and NMDA receptors. This means that the amplitude of the fluctuations of the AMPA synaptic variables will be much larger than

the fluctuations due to GABA or NMDA receptors. Thus, we can neglect the fluctuations due to GABA and NMDA receptors and consider only those corresponding to AMPA receptors. We also neglect $\Delta S_{\mathrm{AMPA,rec}}(t)$ since recurrent imputs are dominated by NMDA and thus $g_{\mathrm{AMPA,rec}}$ is much smaller than $g_{\mathrm{AMPA,ext}}$ in all situations considered here. Thus, the only fluctuating term remaining is $\Delta S_{\mathrm{AMPA,ext}}(t)$. This term can be considered Gaussian, with zero mean and correlation function

$$\langle \Delta S_{\mathrm{AMPA,ext}}(t) \Delta S_{\mathrm{AMPA,ext}}(t') \rangle = C_{\mathrm{ext}} \nu_{\mathrm{ext}} \tau_{\mathrm{AMPA}} \exp\left(-\frac{|t-t'|}{\tau_{\mathrm{AMPA}}} \right).$$

With these approximations, Eq. (1) becomes

$$\begin{aligned} C_{\mathrm{m}} \frac{dV(t)}{dt} = & -g_{\mathrm{m}}(V(t)-V_{\mathrm{L}}) \\ & - g_{\mathrm{AMPA,ext}}(V(t)-V_{\mathrm{E}}) C_{\mathrm{ext}} \tau_{\mathrm{AMPA}} \nu_{\mathrm{ext}} \\ & - g_{\mathrm{AMPA,rec}}(V(t)-V_{\mathrm{E}}) C_{\mathrm{E}} \tau_{\mathrm{AMPA}} \nu_{\mathrm{E}} \\ & - \frac{g_{\mathrm{NMDA}}(V(t)-V_{\mathrm{E}})}{1+\gamma \exp(-\beta V(t))} C_{\mathrm{E}} \psi(\nu_{\mathrm{E}}) \\ & - g_{\mathrm{GABA}}(V(t)-V_{\mathrm{I}}) C_{\mathrm{E}} \tau_{\mathrm{GABA}} \nu_{\mathrm{I}} \\ & - g_{\mathrm{AMPA,ext}}(V(t)-V_{\mathrm{E}}) \Delta S_{\mathrm{AMPA,ext}}(t). \end{aligned} \tag{6}$$

As an additional simplification, we approximate the voltage term by its average $\langle V \rangle$ in the fluctuation term.

Approximation 2: Gating Variable of NMDA Channels as a Function of Presynaptic Rates. The calculation of this function can be done exactly when the input spike train is Poissonian (details can be obtained from the authors on request). The result is

$$\psi(\nu) = \frac{\nu \tau_{\mathrm{NMDA}}}{1+\nu \tau_{\mathrm{NMDA}}} \left(1 + \frac{1}{1+\nu \tau_{\mathrm{NMDA}}} \times \sum_{n=1}^{\infty} \frac{(-\alpha \tau_{\mathrm{NMDA,rise}})^n T_n}{(n+1)!} \right)$$

in which ν is the presynaptic rate, $\tau_{\mathrm{NMDA}} = \alpha \tau_{\mathrm{NMDA,rise}} \tau_{\mathrm{NMDA,decay}}$, and

$$T_n = \sum_{k=0}^{n} (-1)^k \binom{n}{k} \times \frac{\tau_{\mathrm{NMDA,rise}}(1+\nu \tau_{\mathrm{NMDA}})}{\tau_{\mathrm{NMDA,rise}}(1+\nu \tau_{\mathrm{NMDA}}) + k \tau_{\mathrm{NMDA,decay}}}.$$

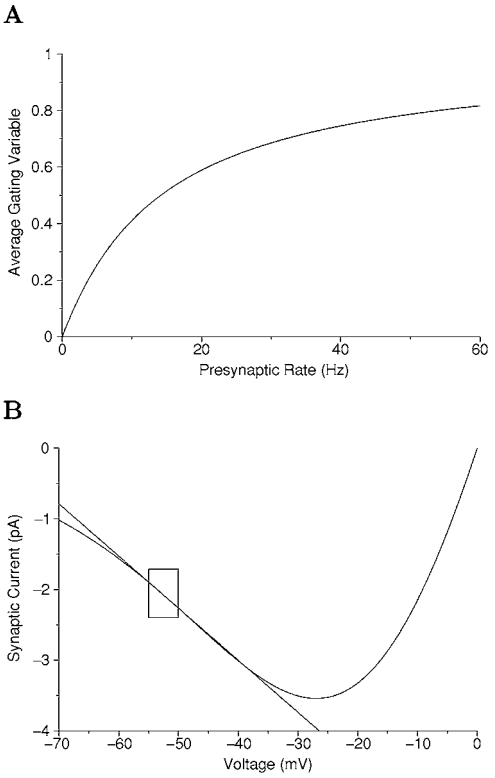

Figure 11. **A:** Time-averaged gating variable of NMDA channels $\psi(\nu)$ as a function of presynaptic spike rate ν. **B:** Current-voltage relationship of NMDA channels and linearization around mean membrane potential (taken here to be −52.5 mV). The box indicates the area where membrane potential spends most of the time. The linear current-voltage relationship is a very good approximation of the Jahr-Stevens formula in that voltage range.

This function is plotted in Fig. 11A. This relationship between the presynaptic rate and the gating variable of NMDA channels is valid strictly speaking for Poissonian input spike trains. We use nonetheless that relationship as a first approximation in the mean-field analysis. We expect it to be very accurate in the spontaneous activity state, where spike trains are very close to Poisson, and slighlty less accurate in persistent activity states, where variability of ISIs is smaller.

Approximation 3: Linearizing the Voltage Dependence of the NMDA Conductance. The NMDA conductance versus voltage relationship can be linearized around the mean value of the voltage $\langle V \rangle$ that will be calculated self-consistently in the following. This is justified if the voltage stays most of the time in a restricted interval around the mean voltage, which is the case in the situations considered in this article.

Indeed, the mean voltage is typically somewhere between the reset potential at −55 mV and the threshold at −50 mV, and the potential stays most of the time between these two values. The linearization gives

$$\frac{V(t)-V_{\mathrm{E}}}{1+\gamma\exp(-\beta V(t))} \approx \frac{V(t)-V_{\mathrm{E}}}{J} + \beta\frac{(V(t)-\langle V\rangle)(\langle V\rangle - V_{\mathrm{E}})(J-1)}{J^2}, \quad (7)$$

where we have neglected the quadratic terms in $V(t)-\langle V\rangle$ and defined $J = 1+\gamma\exp(-\beta\langle V\rangle)$. We show in Fig. 11B the voltage dependence of the NMDA current together with the linearization close to the average potential. It shows that the linearized form gives a good approximation in the region of interest.

With this second set of approximations, Eq. (6) can be simplified to

$$\tau_{\mathrm{E}}\frac{dV(t)}{dt} = -(V(t)-V_{\mathrm{L}}) + \mu_{\mathrm{E}} + \sigma_{\mathrm{E}}\sqrt{\tau_{\mathrm{E}}}\eta(t), \quad (8)$$

where

$$\tau_{\mathrm{E}} = \frac{C_{\mathrm{m}}}{g_{\mathrm{m}}S_{\mathrm{E}}} \quad (9)$$

$$S_{\mathrm{E}} = 1 + T_{\mathrm{E,ext}}\nu_{\mathrm{ext}} + T_{\mathrm{E,AMPA}}\nu_{\mathrm{E}} + (\rho_1+\rho_2)\psi(\nu_{\mathrm{E}}) + T_{\mathrm{EI}}\nu_{\mathrm{I}} \quad (10)$$

$$\mu_{\mathrm{E}} = \frac{(T_{\mathrm{E,ext}}\nu_{\mathrm{ext}} + T_{\mathrm{E,AMPA}}\nu_{\mathrm{E}} + \rho_1\psi(\nu_{\mathrm{E}}))(V_{\mathrm{E}}-V_{\mathrm{L}})}{S_{\mathrm{E}}} + \frac{\rho_2\psi(\nu_{\mathrm{E}})(\langle V\rangle - V_{\mathrm{L}}) + T_{\mathrm{EI}}\nu_{\mathrm{I}}(V_{\mathrm{I}}-V_{\mathrm{L}})}{S_{\mathrm{E}}} \quad (11)$$

$$\sigma_{\mathrm{E}}^2 = \frac{g_{\mathrm{AMPA,ext}}^2(\langle V\rangle - V_{\mathrm{E}})^2 C_{\mathrm{ext}}\nu_{\mathrm{ext}}\tau_{\mathrm{AMPA}}^2\tau_{\mathrm{E}}}{g_{\mathrm{m}}^2\tau_{\mathrm{m}}^2} \quad (12)$$

$$\langle\eta(t)\rangle = 0 \quad (13)$$

$$\langle\eta(t)\eta(t')\rangle = \frac{1}{\tau_{\mathrm{AMPA}}}\exp\left(-\frac{|t-t'|}{\tau_{\mathrm{AMPA}}}\right) \quad (14)$$

$$T_{\mathrm{E,ext}} = \frac{g_{\mathrm{AMPA,ext}}C_{\mathrm{ext}}\tau_{\mathrm{AMPA}}}{g_{\mathrm{m}}} \quad (15)$$

$$T_{\mathrm{E,AMPA}} = \frac{g_{\mathrm{AMPA,rec}}C_{\mathrm{E}}\tau_{\mathrm{AMPA}}}{g_{\mathrm{m}}} \quad (16)$$

$$\rho_1 = \frac{g_{\mathrm{NMDA}}C_{\mathrm{E}}}{g_{\mathrm{m}}J} \quad (17)$$

$$\rho_2 = \beta\frac{g_{\mathrm{NMDA}}C_{\mathrm{E}}(\langle V\rangle - V_{\mathrm{E}})(J-1)}{g_{\mathrm{m}}J^2} \quad (18)$$

$$T_{\mathrm{EI}} = \frac{g_{\mathrm{GABA}}C_{\mathrm{I}}\tau_{\mathrm{GABA}}}{g_{\mathrm{m}}}. \quad (19)$$

τ_{E} is the effective membrane time constant. It is decreased compared to the bare membrane time constant $C_{\mathrm{m}}/g_{\mathrm{m}}$ by the shunting factor S_{E} due to the conductance increase due to the various types of synaptic bombardments. μ_{E} is the asymptotic value the membrane potential would have in the absence of fluctuations and in the absence of spiking. Last, σ_{E} measures the magnitude of the fluctuations in the synaptic inputs. η is a Gaussian process with an exponentially decaying correlation function with time constant τ_{AMPA}. The other factors describe the impact of the firing of the different population to both shunting factor and μ_{E}.

The discharge rate of a cell whose potential is described by Eq. (8) with a noise term with correlation time τ_{AMPA} has been obtained in the limit $\tau_{\mathrm{AMPA}} \ll \tau_{\mathrm{E}}$ by Brunel and Sergi (1998). The result is

$$\nu_{\mathrm{E}} = \phi(\mu_{\mathrm{E}}, \sigma_{\mathrm{E}}), \quad (20)$$

where

$$\phi(\mu_{\mathrm{E}}, \sigma_{\mathrm{E}}) = \left(\tau_{\mathrm{rp}} + \tau_{\mathrm{E}}\int_{\beta(\mu_{\mathrm{E}},\sigma_{\mathrm{E}})}^{\alpha(\mu_{\mathrm{E}},\sigma_{\mathrm{E}})} \times du\sqrt{\pi}\exp(u^2)[1+\mathrm{erf}(u)]\right)^{-1} \quad (21)$$

$$\alpha(\mu_{\mathrm{E}}, \sigma_{\mathrm{E}}) = \frac{(V_{\mathrm{thr}}-V_{\mathrm{L}}-\mu_{\mathrm{E}})}{\sigma_{\mathrm{E}}}\left(1+0.5\frac{\tau_{\mathrm{AMPA}}}{\tau_{\mathrm{E}}}\right) + 1.03\sqrt{\frac{\tau_{\mathrm{AMPA}}}{\tau_{\mathrm{E}}}} - 0.5\frac{\tau_{\mathrm{AMPA}}}{\tau_{\mathrm{E}}} \quad (22)$$

$$\beta(\mu_{\mathrm{E}}, \sigma_{\mathrm{E}}) = \frac{V_{\mathrm{reset}}-V_{\mathrm{L}}-\mu_{\mathrm{E}}}{\sigma_{\mathrm{E}}}. \quad (23)$$

ϕ describes how the discharge rate varies as a function of parameters defining the statistical properties of the membrane potential in presence of synptic inputs. It can be considered as a f-I curve generalized to a noisy situation, where μ plays the role of the average current.

The average membrane potential can be calculated from the distribution of potentials obtained in Brunel and Hakim, (1999). The result is

$$\langle V\rangle = \mu_{\mathrm{E}} - (V_{\mathrm{thr}}-V_{\mathrm{reset}})\nu_{\mathrm{E}}\tau_{\mathrm{E}}. \quad (24)$$

Interneurons are described by similar equations, replacing index E by I everywhere and using the appropriate single-cell parameters.

Structured Activity

In the event of persistent activity, the network of pyramidal cells breaks in three subpopulations: neurons selective for the shown stimulus, described by an index *act*; cells activated by other stimuli (+); cells activated by none of the stimuli (0).

These populations are now described by

$$S_{\rm act} = 1 + T_{\rm E,ext}\nu_{\rm ext} + T_{\rm E,AMPA}n_{\rm act} + (\rho_1+\rho_2)N_{\rm act} + T_{\rm EI}\nu_{\rm I} \quad (25)$$

$$\mu_{\rm act} = \frac{(T_{\rm E,ext}\nu_{\rm ext} + T_{\rm E,AMPA}n_{\rm act} + \rho_1 N_{\rm act})V_{\rm E} + \rho_2 N_{\rm act}\langle V\rangle + T_{\rm EI}\nu_{\rm I}V_{\rm I}}{S_{\rm act}} \quad (26)$$

$$S_{+} = 1 + T_{\rm E,ext}\nu_{\rm ext} + T_{\rm E,AMPA}n_{+} + (\rho_1+\rho_2)N_{+} + T_{\rm EI}\nu_{\rm I} \quad (27)$$

$$\mu_{+} = \frac{(T_{\rm E,ext}\nu_{\rm ext} + T_{\rm E,AMPA}n_{+} + \rho_1 N_{+})V_{\rm E} + \rho_2 N_{+}\langle V\rangle + T_{\rm EI}\nu_{\rm I}V_{\rm I}}{S_{+}} \quad (28)$$

$$S_{0} = 1 + T_{\rm E,ext}\nu_{\rm ext} + T_{\rm E,AMPA}\nu_{\rm E} + (\rho_1+\rho_2)N_{\rm E} + T_{\rm EI}\nu_{\rm I} \quad (29)$$

$$\mu_{0} = \frac{(T_{\rm E,ext}\nu_{\rm ext} + T_{\rm E,AMPA}\nu_{\rm E} + \rho_1 N_{\rm E})V_{\rm E} + \rho_2\psi(\nu_{\rm E})\langle V\rangle + T_{\rm EI}\nu_{\rm I}V_{\rm I}}{S_{0}}, \quad (30)$$

where

$$n_{\rm act} = f w_{+}\nu_{\rm act} + f(p-1)w_{-}\nu_{+} + (1-fp)w_{-}\nu_{0} \quad (31)$$

$$N_{\rm act} = f w_{+}\psi(\nu_{\rm act}) + f(p-1)w_{-}\psi(\nu_{+}) + (1-fp)w_{-}\psi(\nu_{0}) \quad (32)$$

$$n_{+} = f w_{-}\nu_{\rm act} + f(w_{+}+(p-2)w_{-})\nu_{+} + (1-fp)w_{-}\nu_{0} \quad (33)$$

$$N_{+} = f w_{-}\psi(\nu_{\rm act}) + f(w_{+}+(p-2)w_{-})\psi(\nu_{+}) + (1-fp)w_{-}\psi(\nu_{0}) \quad (34)$$

$$\nu_{\rm E} = f\nu_{\rm act} + f(p-1)\nu_{+} + (1-fp)\nu_{0} \quad (35)$$

$$N_{\rm E} = f\psi(\nu_{\rm act}) + f(p-1)\psi(\nu_{+}) + (1-fp)\psi(\nu_{0}). \quad (36)$$

The mean frequencies in each of these three populations are given by Eqs. (20) to (23) in which the above equations have to be inserted. As a result we get a system of four coupled nonlinear equations to be solved to obtain $\nu_{\rm act}$, ν_{+}, ν_0, and $\nu_{\rm I}$.

Solving Numerically the Mean-Field Equations

Firing Rates as a Function of Network Parameters. The mean-field equations giving the firing rates in the four neuronal populations are of the form of Eq. (20) for each population—that is,

$$\nu_{\rm act} = \phi(\mu_{\rm act}, \sigma_{\rm E}) \quad (37)$$

$$\nu_{+} = \phi(\mu_{+}, \sigma_{\rm E}) \quad (38)$$

$$\nu_{0} = \phi(\mu_{0}, \sigma_{\rm E}) \quad (39)$$

$$\nu_{\rm I} = \phi(\mu_{\rm I}, \sigma_{\rm I}), \quad (40)$$

where ϕ, the f-I curve, is given by Eqs. (21) to (23), the mean voltages due to synaptic inputs μ are given by Eqs. (25) to (30), and the amplitude of the synaptic noise by Eq. (12). Note that the μ's depend on all discharge rates ν's through Eqs. (25) to (30), while the σ's also depend on the discharge rates through the mean voltages given by Eq. (24). Thus, Eqs. (37) to (40) form a close system of nonlinear equations to be solved to obtain discharge rates of all populations in a stationary state of the network.

To solve these equations, we use first-order differential equations whose fixed point solutions correspond to the solutions of Eqs. (37) to (40):

$$\tau_{\rm E}\frac{d\nu_{\rm act}}{dt} = -\nu_{\rm act} + \phi(\mu_{\rm act}, \sigma_{\rm E}) \quad (41)$$

$$\tau_{\rm E}\frac{d\nu_{+}}{dt} = -\nu_{+} + \phi(\mu_{+}, \sigma_{\rm E}) \quad (42)$$

$$\tau_{\rm E}\frac{d\nu_{0}}{dt} = -\nu_{0} + \phi(\mu_{0}, \sigma_{\rm E}) \quad (43)$$

$$\tau_{\rm I}\frac{d\nu_{\rm I}}{dt} = -\nu_{\rm I} + \phi(\mu_{\rm I}, \sigma_{\rm I}). \quad (44)$$

Similar equations are often used in neural network modeling for describing the dynamics of firing-rate neurons (e.g., Wilson and Cowan, 1973).

These equations are solved by standard numerical integration techniques (Press et al., 1992), using different initial conditions. To obtain spontaneous activity solutions ($\nu_{\rm act} = \nu_{+} = \nu_0$) we start with $\nu_{\rm act} = \nu_{+} = \nu_0$. To obtain working memory solutions ($\nu_{\rm act} > \nu_{+}$) we start with an initial condition $\nu_{\rm act} \gg \nu_{+}$. Finally, to obtain the boundaries of the basins of attraction of spontaneous and working memory solutions, we proceed iteratively with $\nu_{\rm act}$ between its spontaneous and persistent activity values. For a given $\nu_{\rm act}$, we run the dynamics of the remaining populations *at fixed* $\nu_{\rm act}$ until an equilibrium is reached (for similar considerations, see Mascaro and Amit, 1999). Then we observe whether the dynamics flows toward the spontaneous or persistent activity fixed points. Then we find iteratively the value of $\nu_{\rm act}$ that limits the basins of attraction of both states.

Network Parameters as a Function of Firing Rates. In the simulations, we have chosen to determine synaptic conductances in order for the network to have a prescribed level of spontaneous activity, ν_E for pyramidal cells and ν_I for interneurons. For example, we have calculated the values of the synaptic conductances given in the Methods section such that the network has, in its spontaneous activity state, $\nu_E = 3$ Hz and $\nu_I = 9$ Hz. Of course, there are more synaptic conductances than spontaneous rates (8 versus 2). Thus, we need to provide additional constraints. The constraints we choose are the following: (1) the average external excitatory inputs are taken to be equal to the average recurrent excitatory inputs; (2) the fraction of NMDA receptors in recurrent excitatory synaptic inputs in terms of charge entry per spike at mean voltage is fixed to 0.95; (3) the ratio of the mean recurrent inhibition to mean recurrent excitation is fixed, in terms of charge entry per spike at mean voltage, to $R = 3$. Since there are three constraints for both pyramidal cells and interneurons, this gives the needed six constraints that allows to determine the synaptic conductances. As a result of solving the mean-field equations in this way, we obtain the parameters given in the Methods section.

Acknowledgments

N.B. was supported by CNRS, and X.-J.W. was supported by the NSF (IBN-9733006). We also thank the A.P. Sloan Foundation and the W.M. Keck Foundation for partial support. We thank D.J. Amit for helpful comments on a previous version of the manuscript and A. Compte and J. Tegner for useful discussions.

References

Abeles M (1991) *Corticonics*. Cambridge University Press, New York.

Amit DJ (1995) The Hebbian paradigm reintegrated: Local reverberations as internal representations. *Behav. Brain Sci.* 18:617.

Amit DJ, Brunel N (1997) Model of global spontaneous activity and local structured activity during delay periods in the cerebral cortex. *Cerebral Cortex* 7:237–252.

Arnsten AFT (1998) Catecholamine modulation of prefrontal cortical cognitive function. *Trends in Cognitive Sciences* 2:436–447.

Braitenberg V, Schütz A (1991) *Anatomy of the Cortex*. Springer-Verlag: Berlin.

Brozoski TJ, Brown RM, Rosvold HE, Goldman PS (1979) Cognitive deficit caused by regional depletion of dopamine in prefrontal cortex of rhesus monkey. *Science* 205:929–932.

Brunel N (2000) Persistent activity and the single cell f-I curve in a cortical network model. *Network* 11:261–280.

Brunel N, Carusi F, Fusi S (1998) Slow stochastic Hebbian learning of classes in recurrent neural networks. *Network* 9:123–152.

Brunel N, Hakim V (1999) Fast global oscillations in networks of integrate-and-fire neurons with low firing rates. *Neural Comput.* 11:1621–1671.

Brunel N, Sergi S (1998) Firing frequency of integrate-and-fire neurons with finite synaptic time constants. *J. Theor. Biol*: 195:87–95.

Burns BD, Webb AC (1976) The spontaneous activity of neurons in the cat's cerebral cortex. *Proc. R. Soc. Lond. B* 194:211–223.

Cai JX, Anrsten AFT (1997) Dose-dependent effects of the dopamine D1 receptor agonists A77636 or SKF81297 on spatial working memory in aged monkeys. *J. Pharmacol. Exp. Ther.* 282:1–7.

Camperi M, Wang XJ (1998) A model of visuospatial short-term memory in prefrontal cortex: Recurrent network and cellular bistability. *J. Comput. Neurosci.* 5:383–405.

Cepeda C, Levine MS (1998) Dopamine and N-methyl-D-aspartate receptor interactions in the neostriatum. *Dev. Neurosci*. 20:1–18.

Cepeda C, Radisavljevic Z, Peacock W, Levine MS, Buchwald NA (1992) Differential modulation by dopamine of responses evoked by excitatory amino acids in human cortex. *Synapse* 11:330–341.

Compte A, Brunel N, Goldman-Rakic PS, Wang XJ (2000) Synaptic mechanisms and network dynamics underlying spatial working memory in a cortical network model. *Cerebral Cortex* 10:910–923.

Condé F, Jacobowitz DM, Baimbridge KG, Lewis DA (1994) Local circuit neurons immunoreactive for calretinin, calbindin D-28k or parvalbumin in monkey prefrontal cortex: Distribution and morphology. *J. Comp. Neurol.* 341:95–116.

Daniel DG, Weinberger DR, Jones DW, Zigun JR, Coppola R, Handel S, Bigelow LB, Goldberg TE, Berman KF, Kleinman JE (1991) The effect of amphetamine on regional cerebral blood flow during cognitive activation in schizophrenia. *J. Neurosci.* 11: 1907–1917.

Destexhe A, Mainen ZF, Sejnowski TJ (1998) Kinetic models of synaptic transmission. In: Koch C, Segev I, eds. *Methods in Neuronal Modeling* (2nd ed.). MIT Press, Cambridge, MA. pp. 1–25.

Douglas RJ, Koch C, Mahowald M, Martin KM, Suarez HH (1995) Recurrent excitation in neocortical circuits. *Science* 269:981–985.

Durstewitz D, Kelc M, Güntürkun O (1999) A neurocomputational theory of the dopaminergic modulation of working memory functions. *J. Neurosci.* 19:2807–2822.

Durstewitz D, Seamans JK, Sejnowski TJ (2000) Dopamine-mediated stabilization of delay-period activity in a network model of prefrontal cortex. *J. Neurophysiol.* 83:1733–1750.

Egan MF, Weinberger DR (1997) Neurobiology of schizophrenia. *Curr. Opin. Neurobiol.* 7:701–707.

Funahashi S, Bruce CJ, Goldman-Rakic PS (1989) Mnemonic coding of visual space in the monkey's dorsolateral prefrontal cortex. *J. Neurophysiol.* 61:331–349.

Fuster JM, Alexander G (1971) Neuron activity related to short-term memory. *Science* 173:652–654.

Fuster JM, Jervey JP (1981) Inferotemporal neurons distinguish and retain behaviourally relevant features of visual stimuli. *Science* 212:952–955.

Gabbott PLA, Bacon SJ (1996) Local circuit neurons in the medial prefrontal cortex (areas 24a,b,c, 25 and 32) in the monkey. *J. Comp. Neurol.* 364:567–636.

Gellman RL, Aghajanian GK (1993) Pyramidal cells in piriform cortex receive a convergence of inputs from monoamine activated GABAergic interneurons. *Brain Res.* 600:63–73.

Goldman-Rakic PS (1987) Circuitry of primate prefrontal cortex and regulation of behavior by representational memory. In: *Handbook of Physiology: The Nervous System V.* American Physiological Society, Bethesda, MD. Chapter 9, pp. 373–417.

Goldman-Rakic PS (1994) Working memory dysfunction in schizophrenia. *J. Neuropsych. and Clin. Neurosci.* 6:348–357.

Goldman-Rakic PS (1995) Cellular basis of working memory. *Neuron* 14:477–485.

Hansel D, Mato G, Meunier C, Neltner L (1998) On numerical simulations of integrate-and-fire neural networks. *Neural Comput.* 10:467–483.

Hebb DO (1949) *Organization of Behavior*. Wiley, New York.

Hestrin S, Sah P, Nicoll R (1990) Mechanisms generating the time course of dual component excitatory synaptic currents recorded in hippocampal slices. *Neuron* 5:247–253.

Jahr CE, Stevens CF (1990) Voltage dependence of NMDA-activated macroscopic conductances predicted by single-channel kinetics. *J. Neurosci*. 10:3178–3182.

Kawaguchi Y (1997) Selective cholinergic modulation of cortical GABAergic cell subtypes. *J. Neurophysiol*. 78:1743–1747.

Koch KW, Fuster JM (1989) Unit activity in monkey parietal cortex related to haptic perception and temporary memory. *Exp. Brain Res*. 76:292–306.

Kubota K, Niki H (1971) Prefrontal cortical unit activity and delayed alternation performance in monkeys. *J. Neurophysiol*. 34:337–347.

Law-Tho D, Hirsch JC, Crepel F (1994) Dopamine modulation of synaptic transmission in rat prefrontal cortex: An in vitro electrophysiological study. *Neurosci. Res*. 21:151–160.

Lorente de Nó R (1933) Vestibulo-ocular reflex arc. *Arch. Neurol. Psych*. 30:245–291.

Mascaro M, Amit DJ (1999) Effective neural response function for collective population states. *Network* 10:351–373.

McCormick D, Connors B, Lighthall J, Prince D (1985) Comparative electrophysiology of pyramidal and sparsely spiny stellate neurons in the neocortex. *J. Neurophysiol*. 54:782–806.

Miller EK, Erickson CA, Desimone R (1996) Neural mechanisms of visual working memory in prefrontal cortex of the macaque. *J. Neurosci*. 16:5154–5167.

Miyashita Y (1988) Neuronal correlate of visual associative long-term memory in the primate temporal cortex. *Nature* 335:817–820.

Miyashita Y, Chang HS (1988) Neuronal correlate of pictorial short-term memory in the primate temporal cortex. *Nature* 331:68–70.

Muly III EC, Szigeti K, Goldman-Rakic PS (1998) D1 receptor in interneurons of macaque prefrontal cortex: Distribution and subcellular localization. *J. Neurosci*. 18:10553–10565.

Murray JD (1993) *Mathematical Biology*. Springer-Verlag, Berlin.

Nakamura K, Kubota K (1995) Mnemonic firing of neurons in the monkey temporal pole during a visual recognition memory task. *J. Neurophysiol*. 74:162–178.

Nicola SM, Surmeier DJ, Malenka RC (2000) Dopaminergic modulation of neuronal excitability in the striatum and nucleus accumbens. *Ann. Rev. Neurosci*. 23:185–215.

Okubo Y, Suhara T, Suzuki K, Kobayashi K, Inoue O, Terasaki O, Someya Y, Sassa T, Sudo Y, Matsushima E, Iyo M, Tateno Y, Toru M (1997) Decreased prefrontal dopamine D1 receptors in schizophrenia revealed by PET. *Nature* 385:634–636.

Penit-Soria J, Audinat E, Crepel F (1987) Excitation of rat prefrontal cortical neurons by dopamine: An in vitro electrophysiological study. *Brain Res*. 425:263–274.

Pinto DJ, Brumberg JC, Simons DJ, Ermentrout GB (1996) A quantitative population model of whisker barrels: Re-examining the Wilson-Cowan equations. *J. Comput. Neurosci*. 3:247–264.

Press WH, Teukolsky SA, Vetterling WT, Flannery BP (1992) *Numerical Recipes in C*. Cambridge University Press, Cambridge.

Rao SG, Williams GV, Goldman-Rakic PS (1999) Isodirectional tuning of adjacent interneurons and pyramidal cells during working memory: Evidence for microcolumnar organization in PFC. *J. Neurophysiol*. 81:1903–1916.

Salin PA, Prince DA (1996) Spontaneous $GABA_A$ receptor mediated inhibitory currents in adult rat somatosensory cortex. *J. Neurophysiol*. 75:1573–1588.

Sawaguchi T, Goldman-Rakic PS (1991) D1 dopamine receptors in prefrontal cortex: Involvement in working memory. *Science* 251:947–950.

Sawaguchi T, Matsumara M, Kubota K (1990) Catecholaminergic effects on neuronal activity related to a delayed response task in monkey prefrontal cortex. *J. Neurophysiol*. 63:1385–1400.

Servan-Schreiber D, Printz H, Cohen JD (1990) A network model of catecholamine effects: gain, signal-to-noise ratio, and behavior. *Science* 249:892–895.

Shadlen MN, Newsome WT (1994) Noise, neural codes and cortical organization. *Current Opinion in Neurobiol*. 4:569–579.

Somers DC, Nelson SB, Sur M (1995) An emergent model of orientation selectivity in cat visual cortical simple cells. *J. Neurosci*. 15:5448–5465.

Spruston N, Jonas P, Sakmann B (1995) Dendritic glutamate receptor channel in rat hippocampal CA3 and CA1 pyramidal neurons. *J. Physiol*. 482:325–352.

Troyer TW, Krukowski AE, Priebe NJ, Miller KD (1998) Contrast-invariance orientation tuning in cat visual cortex: Thalamocortical input tuning and correlation-based intracortical connectivity. *J. Neurosci*. 18:5908–5927.

Tsodyks MV, Sejnowski T (1995) Rapid state switching in balanced cortical network models. *Network* 6:111–124.

Tuckwell HC (1988) *Introduction to Theoretical Neurobiology*. Cambridge University Press, Cambridge.

Umemiya M, Raymond LA (1997) Dopaminergic modulation of excitatory postsynaptic currents in rat neostriatal neurons. *J. Neurophysiol*. 78:1248–1255.

van Vreeswijk C, Sompolinsky H (1996) Chaos in neuronal networks with balanced excitatory and inhibitory activity. *Science* 274:1724–1726.

Wang XJ (1999) Synaptic basis of cortical persistent activity: The importance of NMDA receptors to working memory. *J. Neurosci*. 19:9587–9603.

Williams GV, Goldman-Rakic PS (1995) Modulation of memory fields by dopamine D1 receptors in prefrontal cortex. *Nature* 376:572–575.

Wilson FAW, Scalaidhe SPO, Goldman-Rakic PS (1993) Dissociation of object and spatial processing domains in primate prefrontal cortex. *Science* 260:1955–1958.

Wilson FAW, Scalaidhe SPO, Goldman-Rakic PS (1994) Functional synergism between putative γ-aminobutyrate-containing neurons and pyramidal neurons in prefrontal cortex. *Proc. Natl. Acad. Sci. USA* 91:4009–4013.

Wilson HR, Cowan JD (1973) A mathematical theory of the functional dynamics of cortical and thalamic nervous tissue. *Kybernetik* 13:55–80.

Xiang Z, Huguenard JR, Prince DA (1998) $GABA_A$ receptor mediated currents in interneurons and pyramidal cells of rat visual cortex. *J. Physiol*. 506:715–730.

Yakovlev V, Fusi S, Berman E, Zohary E (1998) Inter-trial neuronal activity in inferior temporal cortex: A putative vehicle to generate long-term visual associations. *Nature Neurosci*. 1:310–317.

Yang CR, Seamans JK, Gorelova N (1996) Electrophysiological and morphological properties of layer V-VI principal pyramidal cells in rat prefrontal cortex in vitro. *J. Neurosci*. 16:1904–1921.

Zahrt J, Taylor JR, Mathew RG, Arnsten AFT (1997) Supranormal stimulation of D1 dopamine receptors in the rodent prefrontal cortex impairs spatial working memory performance. *J. Neurosci*. 17:8528–8535.

Zheng P, Zhang XX, Bunney BS, Zhi WX (1999) Opposite modulation of cortical N-methyl-D-aspartate receptor-mediated responses by low and high concentrations of dopamine. *Neuroscience* 91:527–535.

Zhou FM, Hablitz JJ (1999) Dopamine modulation of membrane and synaptic properties of interneurons in rat cerebral cortex. *J. Neurophysiol*. 81:967–976.